Quantum dynamics in continuum for proton channel transport

Duan Chen[1] and Guo-Wei Wei[1,2] *

[1] *Department of Mathematics, Michigan State University, East Lansing, MI 48824, USA*

[2] *Department of Electrical and Computer Engineering, Michigan State University, East Lansing, MI 48824, USA*

October 28, 2010

Abstract

Proton transport across membrane is one of the most important and interesting phenomena in living cells. The present work proposes a multiscale/multiphysical model for the understanding of atomic level mechanism of proton transport in transmembrane proteins. We describe proton dynamics quantum mechanically via a density functional approach while implicitly model numerous solvent molecules as a dielectric continuum to reduce the number of degrees of freedom. The density of all other ions in the solvent are assumed to obey the Boltzmann distribution. The impact of protein molecular structure and its charge polarization to the proton transport is considered explicitly in atomic detail. We formulate a total free energy functional to put proton kinetic and potential energies as well as electrostatic energy of all ions on an equal footing. The variational principle is employed to derive nonlinear governing equations for the proton channel system. Generalized Poisson-Boltzmann equation and Kohn-Sham equation are obtained from the variational framework. Theoretical formulations for the proton density and proton channel conductance are constructed based on fundamental principles. The molecular surface of the channel protein is utilized to split the discrete protein domain and the continuum solvent domain, and facilitate the multiscale discrete/continuum/quantum descriptions. A number of mathematical algorithms, including the Dirichlet to Neumann mapping, matched interface and boundary method, Gummel iteration, and Krylov space techniques are utilized to implement the proposed model in a computationally efficient manner. The Gramicidin A (GA) channel is used to demonstrate the performance of the proposed proton channel model and validate the efficiency of the proposed mathematical algorithms. The electrostatic characteristics of the GA channel is analyzed with a wide range of model parameters. The proton channel conductances are studied over a number of applied voltages and reference concentrations. A comparison with experimental data verifies the present model predictions and validates the proposed model.

Keywords: Ion channels, Proton transport, Quantum dynamics in continuum, Multiscale model, Poisson-Boltzmann equation, Kohn-Sham equation, Variational principle.

*Corresponding author. Tel: (517)353 4689, Fax:(517)432 1562, Email: wei@math.msu.edu

Contents

I Introduction

There are a couple of seemingly conflicting fundamental requirements for a living cell to survive and function properly: On the one hand, the cell needs the protection of the plasma membrane, which works as a potential barrier and maintains the intracellular electrolyte composition that may be different from that of the extracellular environment. On the other hand, information communication and material exchange must be established between the intracellular and extracellular environments for all living cells. A wide variety of biological processes, such as signal transduction, nerve impulse and so on, are modulated and sometimes, initiated by the intro/extra-cellular information and material exchanges. These two conflicting tasks are accomplished by ion channels, which are proteins with pores and embedded in lipid bilayers, selectively permitting the permeation of specific ions. Because of these important biological roles, as well as frequently serving the target for drug designing, ion channels have attracted great research interest in experimental, theoretical and computational explorations. Most research activities are focused on a few ion channel properties:[30] (i) The gating of ion channels. Ion channels are not always open or close, based on the mechanism controlling the open/close status, they are categorized as ligand-gated ion channel (the channel is open only when the specific ligand is bonded to the extracellular receptor domain), voltage-gated ion channel (the channel is open/close by the regulating membrane potential) and other gating channels, such as mechanical, sound, and thermal stimuli. It is worthwhile to point out that the present work does not focus on the ion channel gating mechanism — channels discussed here are all assumed open. (ii) The selectivity of the ion channel. When an ion channel is open, it is not open to all the ion species, only certain ions are impermeable. In this sense, ion channels are also classified by the permeable ions, such as potassium channels, sodium channels, and proton channels, etc. (iii) The efficiency of ion conductance. When an ion channel is open and conducts a specific ion species, the efficiency of ion conductance is of major interest, which is measured by the current-voltage (I-V) curve. Technological advance in the past few decades makes it possible to measure I-V curves through a single channel for a variety of ion channels under physiological conditions. These techniques are considerably empowered by the genetic engineering technology to identify the gating mechanism. (iv) Structural analysis. Many channel protein structures have been discovered by X-ray crystallography, nuclear magnetic resonance (NMR) and cryoelectron microscopy. Channel protein structural information is deposited in the Protein Data Bank (PDB). (v) Theoretical and computational research. Abundant knowledge about ion channels accumulated by experimental means has created an excellent testbed for theoretical modeling and prediction of ion channel transport. Various mathematical/physical models have been proposed for numerical simulations. However, there are still many important theoretical problems in the field.[16] One of the problems concerns the dynamical detail of the ion permeating process. Due to the relative narrowness of the pore size, the ion-water geometry needs to be rearranged in order for the ion to successfully cross the channel. Therefore, the orientation and polarity of water molecules, the interaction between partially dehydrated ions and fixed charges on the protein wall must be significantly different from those under the bath condition. Another problem is the precise role of quantum effects in many proton channels, such as the narrow M2 channels of Influenza A. These problems pose challenges for theoretical/mathematical modelings. Commonly used approaches include molecular dynamics, Brownian dynamics, and the Poisson-Nernst-Planck (PNP) equations. There are a number of excellent reviews[16,25,35,45,46,48] for various theoretical models at a variety of levels of descriptions and approximations.

Molecular dynamics (MD) provides one of the most detailed descriptions in modeling biomolecular systems and there are several user-friendly packages available, such as AMBER,[40] CHARMM,[36] etc. In fact, MD is the only known model which is able to predict the ion selectivity in ion channel modeling. However, the use of MD in modeling ion permeation is still limited. The most significant barrier for MD applications in ion channels is the difficulties of predicting the channel conductance, which is the primary physical observable. Extremely small time step (around 1 or 2 femto seconds) has to be employed in the numerical integration of the Newton's equation to obtain the necessary accuracy because the fast time scale of molecular bond motions. Whereas, a typical channel current (with the magnitude of the order of pico Ampere) corresponds to average transit time of tens of nanoseconds for a single ion.

Therefore, the MD simulation must last around microseconds in order to obtain sufficiently accurate conductance calculations. Due to the total simulation time needed and the necessarily small time step, the MD computation without invoking crude approximations is still not affordable with current computers for accurate conductance prediction. Therefore, the full scale MD simulation of ion channels is not feasible. In practice, it is still very useful for MD simulations to obtain alternative channel configurations, solvent polarizations, diffusion coefficients, etc in assisting other approaches for the transport estimation.[16]

Brownian dynamics (BD)[15] based on the Langevin equation treats ions as explicit particles in the ion channel modeling, while describes the surrounding environments (channel protein and lipid bilayer) implicitly by a continuum approach. In Brownian dynamics, there many forces which act on the target ion.[16] First, there is a force from fixed charges in the protein and membrane, and the applied external field. Additionally, there is a force from the self-induced charge by an ion on the channel boundary. When ions pass through the channel, there is always a repelling force induced at the channel boundary against the ion motion. Finally, there is a force from mobile ions in bath regions. Among three components, the force from fixed charges can be obtained by solving the Poisson equation in the absence of mobile ions, whereas forces due to mobile ions can be evaluated by solving the Poisson equation while switching off fixed charge and applied field, and allowing ions to move around all the grid points. Once these Poisson equations are solved numerically, the forces are pre-stored in the grid and ready to be used to determine ion trajectories.

By assuming a mean-field approximation, the Poisson-Nernst-Planck (PNP) model[52] is a continuum electro-diffusion theory which treats not only the protein, lipid layer, bath solution as continuum, but also the ion of interest. The Poisson equation provides the electrostatic potential profile in the whole computational domain based on charge sources from mobile ions in the solution and fixed charges in the channel protein and lipid layer. The gradient of the electrostatic potential gives rise to the driven force, which, together with the gradient of ion density, is used in the Nernst-Planck equation to determine ion density flux. Therefore, ion density distribution is governed by both the electrostatics induced drifting and the density gradient induce diffusion. The ion conductance is computed from the charge flux. Obviously, both the BD and the PNP models have a number of similarities in their initial setups and computational approaches.[24,37,42]

Due to its computational efficiency, the PNP model has been widely implemented for various ion channels[31–33,57] embedded in different lipid bilayers.[7,32] Many mathematical analyses, for example, derivation of the NP equation from Boltzmann equation via perturbation theory,[52] asymptotic expansions of the I-V relations,[1] accelerating algorithms[23] and inverse problems related to the ion selectivity,[6] are also popular research topics in the field. However, the validity of the PNP model has been questioned in many aspects, particularly for narrow ion channels.[17,29,38] Arguments root from the theoretical defect that ions are treated as continuum instead of particles in the narrow channel. This continuum assumption is only reasonable under bulk concentration condition or a channel pore with a sufficiently large diameter. First of all, it is conceptually difficult to define ion "concentration" when the diameter of a channel pore is comparable to that of an ion. Secondly, when the scale is down to a couple of angstroms, non-electrostatic factors such as Brownian motion, may become important or even dominant. The screening effect is significant when the channel diameter is smaller than the Debye length of the realistic electrolyte. In this situation, ion particles induce dielectric boundary charges, which result in a dielectric self-energy (DSE) barrier. The PNP model neglects these energy barrier factors,[7,16] and usually overestimates biological quantities of interest. In the PNP model ignores the non-electrostatic forces and self-energy, and employs an artificially reduced diffusion coefficient (about a factor of $1/50$) to fit experimental data.[31] Several modified PNP models have been proposed, in which the ion self-energy is obtained either by using the Poisson equation[18,29] or the MD[37] simulation, and is added to the Nernst-Planck equation.

Apart from the ion transport of sodium, potassium and calcium, the long range proton transfer (LRPT) across bio-membranes also is of central importance and plays a major role in many biochemical processes, such as cellular respiration, ATP synthase, photosynthesis and denitrification.[34] The LRPT is usually realized via proton channels or proton nanowires, where water molecules are connected in a chain to conduct protons. Two common examples of proton channels are the Gramicidin A (GA) and

the newly discovered M2 proton channel of Influenza A.[49] Theoretical investigation has been extensively carried out and various experimental data about the proton flux are available.[41–43] However, the main mechanism of the LRPT is not fully understood yet,[53] with the belief that protons are totally different from other ions and have larger conductance. In the Grotthuss-type mechanism theory,[2,39] protons achieve the translocation in the channel through a succession of hops along a single chain of hydrogen-bonded water molecules, i.e., an existing hydrogen bonded network, compared to other ions for which the permeation occurs mainly via hydrodynamic diffusion. The actual transfer through the hydrogen bonded net work is usually fast and both the rearrangement of the hydrogen bonded net work and energy barrier are considered as rate limiting factors. There is an agreement that the aforementioned BD theory and PNP model may be expected to work well for heavy ions but not for protons, which have lighter mass and whose transfer involves the hydrogen bonds making and breaking. These processes need to be studied quantum mechanically. Some investigators have explored proton channels via Feynman path integral simulations and quantum energy levels of protons are computed by the Schrödinger equation.[41–43] Several theoretical models are proposed in the last decade.[5,50,53]

The objective of the present work is to propose a multiscale quantum dynamics in continuum (QDC) model for the prediction and analysis of the proton translocation across transmembrane channels. We describe the dynamics of protons quantum mechanically while represent the density of other ions by the Boltzmann distribution, which is in a quasi-equilibrium due to the change of the electrostatic potential during the proton transmembrane permeating process. Since the van der Waals interactions involve less energy compared to electrostatic ones, the numerous solvent molecules are implicitly treated as a dielectric continuum to reduce the number of degrees of freedom of the system. The impact of protein molecular structure and its fixed charges to the proton transport is explicitly considered in our model. We propose a total free energy framework to put the kinetic and potential energies of protons and the electrostatic energy of the whole system, i.e., all ions, channels protein and lipid bilayer, on an equal footing. By using the variational principle, we derive governing equations of the Poisson-Boltzmann and Kohn-Sham types for the proton channel system. There are a few reasons for us to employ the present quantum mechanical description. First, the proton transport mechanism is different and the hydrodynamic approximation is not valid any more. Secondly, conceptually the ion concentration is no longer well defined in a small-size channel. Instead, the probability density function is used for protons. Moreover, many proton channels are very narrow with extremely small local diameters around 2Å,[49] which implies a strong confinement in the transverse directions. The preliminary results of the present work were reported in a poster elsewhere.[10]

The rest of the present paper is organized as follows. Section II is devoted to the theory and model. We present a variational paradigm for analyzing proton channels. Our model incorporates quantum mechanical treatment of protons, classical description of electrostatics, and atomic detail of protein structure and charges. Formalisms for proton density and transport are derived from fundamental principles. Section III discusses numerical implementation and computational algorithms. The molecular surface[47] is employed to separate the discrete/continuum domains and facilitate the quantum/classical descriptions. To simplify the computation, we adopt a decomposition approximation to split the proton transport direction from the transverse confined directions. Mathematical ingredients of this quantum/discrete/continuum model include coupled nonlinear partial differential equations (PDEs) and the elliptic PDEs with discontinuous coefficients and singular sources. Therefore, the corresponding numerical algorithms, matched interface and boundary (MIB) method, Dirichlet-to-Neumann mapping (DNM) and Krylov space iteration schemes are equipped to implement the numerical simulations. In Section IV, we employ a commonly used proton channel protein, the Gramicidin A (GA), to demonstrate the performance of the proposed theoretical model and validate the proposed computational algorithms. Electrostatic properties are analyzed with a number of combinations of model parameters to gain a basic understanding of the GA channel. The conductance of protons under various external voltages and concentrations are simulated. Comparison is made with experimental measurements in the literature. This paper ends with a brief conclusion.

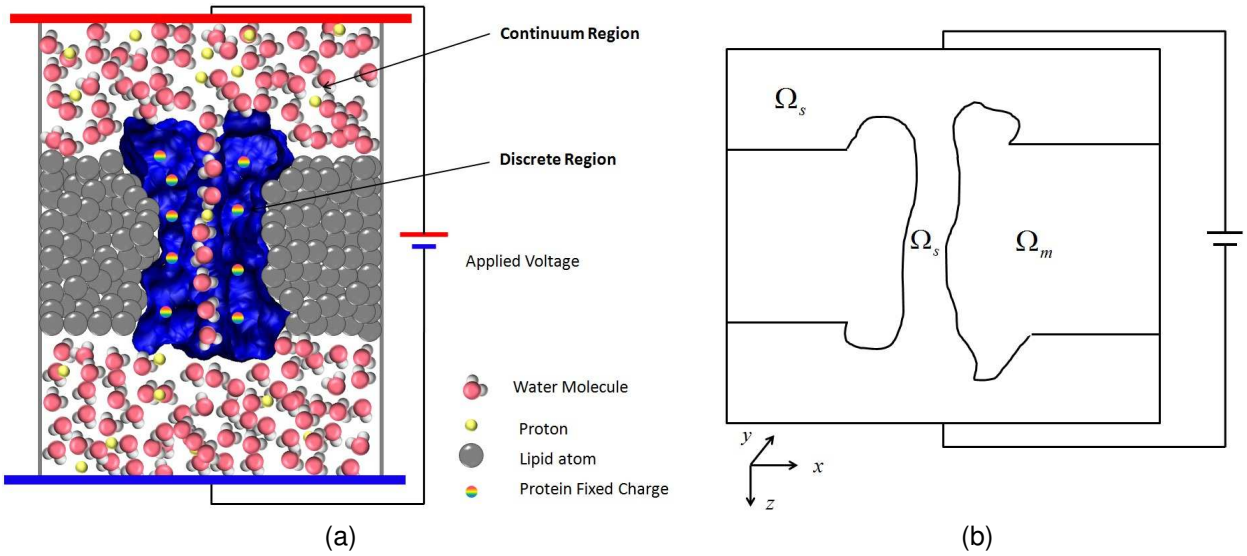

Figure 1: (a) Illustration of multiscale model of a proton channel; (b) Computational domains of the multiscale model with Ω_m being the channel molecule and membrane domain and Ω_s being the solvent domain. Here z-direction is regarded as the transport direction.

II Theory and model

In this section we provide the theoretical formulation of our model of quantum dynamics in continuum.

II.A General description of the model

An ion channel system is complex in terms of biological structure, dynamics and transport. Our goal is to model the dynamics and to predict the transport. To this end, we propose a multiscale, multiphysics and multidomain model. The computational domain Ω is divided into two subdomains, i.e., the solvent domain Ω_s consisting of the extracellular/intracellular solvent regions and the ion channel or channel pore region, and the biomolecular subdomain Ω_m including the membrane protein(s) as well as lipid bilayers. Therefore, we have $\Omega = \Omega_s \cup \Omega_m$. A detailed graph of these subdomains is given in Fig. 1. The interface Γ between solvent-membrane protein is defined by the molecular surface generated by the MSMS software package.[47] It is interesting to note that the physics in each subdomain is very different and there are multiphysics phenomena even in a single subdomain. For the biomolecular subdomain, the membrane protein and lipid bilayer structural data are either generated for molecular dynamics simulations, or downloaded from the Protein Data Bank (PDB) which are collected from X-ray crystallography or nuclear magnetic resonance (NMR) experiments. The force field parameters, such as atomic van der Waals radii and point charges, are obtained from the CHARMM force field.[36] This structural information is utilized in solving the Poisson equation for the electrostatic potential. The electrostatic potential distribution near the channel pore is crucial to the channel selectivity, gating, and ion conductance. The interactions between the channel protein and transmission channel ions are accounted in the present model.

In the solvent subdomain, there are three types of materials, ions of interest (i.e., protons), all other ion species and water molecules. In this system, the charge-charge interactions contribute to the predominate potential energy landscape. Whereas, the strength of other interactions, such as ion-water dipolar interactions, water-water interactions and molecular van der Waals interactions, is much weaker than that of direct charge-charge interactions. This feature provides us a ground to take a multiscale approach to the multiphysics situation in ion channel dynamics. To reduce the number of degrees of freedom, we treat solvent (water) molecules as continuum background or bath. The formation of ion and water clusters and possible ion-water correlations are modeled partly as a dielectric constant effect and partly as a non-electrostatic potential effect. Except for the ions of interest, other ions usually have a small population in the channel pore of a selective channel. Whereas in the bath region, all ions are es-

sentially in a quasi-equilibrium state and their densities are well described by the Boltzmann distribution except for at the solvent-membrane protein interface. Near the solvent-membrane protein interface, the density distribution of ions might be better described by the density functional theory of solution, or integral equations, in which the dispersion interaction between solvent and solute can be better accounted. This effect is modeled as non-electrostatic potential effects in the present work.

The physics in the channel pore region is of central interest and is sharply different from those of other regions. The ions of interest are selected as those which have significant population inside the channel region. There are many evidences which indicate the quantum mechanical behavior of proton transfer in biomolecular systems and proton channels.[4,19] The first reason is the small mass of a proton which enhances the quantum tunneling effect in the proton transport. Additionally, a narrow channel morphology in many proton channels, such as the Influenza A M2 proton channel[11,49] leads to severe quantum confinement, which consequently promotes quantum effects. Finally, hydrogen-bonded chain (proton nanowire) of water molecules assisted proton translocation is quantum mechanical in origin.[41–43] Although theoretical models were proposed in the last decades,[5,50,53] the detailed mechanism of proton dynamics and transport is not fully understood. For these reasons, we treat protons quantum mechanically via a scattering formalism which describes how a quantum mechanical proton scatters through electrostatic and non-electrostatic potential fields. The electrostatic potentials include interactions between protons represented by a self-consistent mean field approximation, the interactions between protons and fixed ions from membrane proteins and lipid bilayers, and the interactions between protons and other ion species. The non-electrostatic potential is due to the impacts of the continuum solvent, the van der Waals interaction between the solvent and biomolecules, the effect of ion-water clusters and possible break-down of hydrogen-bonded chain in a narrow channel, etc. We utilize a total energy functional framework[9,12,54] to incorporate quantum mechanical description and continuum description. Coupled Kohn-Sham equation for the proton dynamics and Poisson-Boltzmann equation for the electrostatic potential are derived from the variational principle. Solutions to these coupled equations give rise to proton structure dynamics, and transport in the ion-channel process, which describes how a quantum mechanical proton scatters through electrostatic and non-electrostatic potential fields. The electrostatic potentials include interactions between protons represented by a self-consistent mean field approximation, the interactions between protons and fixed ions from membrane proteins and lipid bilayers, and the interactions between protons and other ion species. The non-electrostatic potential is due to the impacts of the continuum solvent, the van der Waals interaction between the solvent and biomolecules, the effect of ion-water clusters and possible break-down of hydrogen-bonded chain in a narrow channel, etc. We utilize a total energy functional framework[9,12,54] to incorporate quantum mechanical description and continuum description. Coupled Kohn-Sham equation for the proton dynamics and Poisson-Boltzmann equation for the electrostatic potential are derived from the variational principle. Solutions to these coupled equations give rise to proton structure dynamics, and transport in the ion-channel process.

II.B Free energy components

This subsection describes various free energy components in our multiscale model of quantum dynamics in continuum. In order to give a clear description, Fig. 1(a) is reduced to a sketch in Fig. 1(b) in $x-z$ cross section, where the z direction represents the proton transport direction: the system is restricted to a rectangular cuboid with appropriate size and partitioned into two different computational domains. The permittivity $\epsilon(\mathbf{r})$ has different values in two domains

$$\epsilon(\mathbf{r}) = \begin{cases} \epsilon_s(\mathbf{r}) & \forall \mathbf{r} \in \Omega_s \\ \epsilon_m(\mathbf{r}) & \forall \mathbf{r} \in \Omega_m \end{cases} . \tag{1}$$

Since both the membrane and channel protein are treated with same dielectric medium, the interface between them is erased and a constant dielectric constant is assumed on Ω_m. On the contrast, the solvent in the bath regions and in the channel pore have different biological characteristics. Therefore the position dependent dielectric constant is imposed on the solvent domain Ω_s. In fact, $\epsilon_s(\mathbf{r})$ in the channel region can differ much from that in the bulk region. The detailed discussion about the dielectric

constants is given in Section III.E. There are three major categories of macroscopic variables in the model which are defined in different subdomains and formulated in classical and quantum mechanisms.

II.B.1 Electrostatic free energy in the biomolecular region

The biomolecular region consists of membrane protein and lipid bilayer. Their structures determine the channel selectivity and gating efficiency. In the present treatment, we assume that structures of membrane protein and lipid bilayer are given and do not change during the ion transport process. This is certainly an approximation and will be easily removed in our future work by a combination of the present formulation with MD simulations.[54] Without structural modification, the biomolecules still significantly contribute to ion dynamics and transport by electrostatic interactions. The fixed charges in the channel protein and nearby lipid bilayers determine the fundamental characteristics of the channel and provide the primary environment for ions' permeation. Since the total number of the fixed charges is not too large (i.e., up to thousands), with the assumption that the positions of them are essentially fixed, the explicit discrete description is actually affordable. In this sense, they serve as a source term in the electrostatic potential calculation

$$\rho_f(\mathbf{r}) = \sum_{i=1}^{N_a} Q_i \delta(\mathbf{r} - \mathbf{r}_i) \tag{2}$$

where N_a is the total number of fixed charges, Q_i and $\mathbf{r}_i$ are the point charge and position of the ith atom. Therefore, the electrostatic free energy in biomolecular domain is given by

$$G_{\rm Mol}[\Phi, n] \quad = \quad \int \left[\frac{\epsilon_m(\mathbf{r})}{2} |\nabla \Phi|^2 - \Phi \rho_f \right] d\mathbf{r}, \tag{3}$$

where $\Phi(\mathbf{r})$ is the electrostatic potential and is defined on the whole domain $\Omega_s \cup \Omega_m$.

II.B.2 Electrostatic free energy in the solvent region

The ions in the solvent region also contribute to the electrostatic potential. Protons and other ion species are treated in different manners. Let us denote the proton number density in the solvent region as $n(\mathbf{r})$ and the charge density as $\rho_p = qn(\mathbf{r})$, q is the elementary charge or charge carried by a single proton. The charge density serves as a source term in the electrostatic free energy.

In the solvent region, particularly, in the extracellular and intracellular solvent regions, apart from ions of interest, there are many other ions. In the present model, all other ions are treated in a different manner from the ion of interest. Specifically, no detailed description is given to individual ions except for the ions of interest. However, other ions contribute considerably to the electrostatic property of the whole system. To account for their electrostatic effort, we describe other ions by using the Boltzmann distribution. The charge density of other ions is given by

$$\rho' = \sum_{j}^{N_c'} q_j n_j'(\mathbf{r}) = \sum_{j}^{N_c'} q_j n_j^0 e^{-q_j(\Phi(\mathbf{r}) - V_{\rm Ext})/k_B T}, \tag{4}$$

where N_c' is the total number of other ionic species, n_j^0 and q_j are the bulk constant density and charge of the jth ion species. Here $n_j' = n_j^0 e^{-q_j(\Phi(\mathbf{r}) - V_{\rm Ext})/k_B T}$ is the number density of jth ion species, it can be noticed that the Boltzmann distribution of the other ionic species with respected to the potential has been modified with the generalized chemical potential $V_{\rm Ext}$, which represents the effects of the chemical potential of jth ion species and the external electric field.[44,46]

The corresponding electrostatic free energy in the solvent region is given by

$$G_{\rm Sol}[\Phi] \quad = \quad \int \left[\frac{\epsilon_s(\mathbf{r})}{2} |\nabla \Phi(\mathbf{r})|^2 - \Phi(\mathbf{r}) \rho_p(\mathbf{r}) + k_B T \sum_{j}^{N_c'} n_j^0 \left(e^{-q_j(\Phi(\mathbf{r}) - V_{\rm Ext})/k_B T} - 1 \right) \right] d\mathbf{r}, \tag{5}$$

Note that the electrostatic free energy of other ions in Eq. (5) is similar in spirit to Sharp and Honig,[51] Gilson et al,[28] Chen et al[12] and and Wei.[54]

II.B.3 Proton free energies and interactions

The solvent region might admit a number of ion species, of which a full quantum model can be technically complicated and computationally time consuming. We therefore only treat the ions of interest, i.e., protons, quantum mechanically and assume a continuum description of other ion species. To simplify the problem further, we consider a generalized density functional theory for protons.

Kinetic energy. The proton density operator n_H is given by

$$n_H = e^{-(H-E_{\rm Ext})/k_BT}. \tag{6}$$

where H is the Hamiltonian of the system and $E_{\rm Ext}$ is the external electrical field energy. We define the proton density $n(\mathbf{r})$ as

$$n(\mathbf{r}) = \langle \mathbf{r}|n_H|\mathbf{r}\rangle = \int |\Psi_E(\mathbf{r})|^2 e^{-(E-E_{\rm Ext})/k_BT} dE, \tag{7}$$

where Ψ_E and E are the wavefunction and corresponding energy associated with H. The Boltzmann statistics is adopted in the present work. The kinetic energy is given by $\frac{\mathbf{p}^2}{2m(\mathbf{r})}$ where $\mathbf{p}$ is the momentum and m is proton effective mass. In the coordinate representation, the kinetic energy of protons can be given as

$$\int\int \frac{\hbar^2 e^{-(H-E_{\rm Ext})/k_BT}}{2m(\mathbf{r})} |\nabla \Psi_E(\mathbf{r})|^2 dE d\mathbf{r}, \tag{8}$$

where the Boltzmann factor weights different energy contributions.

Electrostatic potential. Protons have a number of electrostatic interactions. First, protons interact repulsively among themselves

$$U_{\rm Ion-Ion}(\mathbf{r}) = \frac{1}{2}\int \frac{q^2 n(\mathbf{r}) n(\mathbf{r}')}{\epsilon(\mathbf{r})|\mathbf{r}-\mathbf{r}'|} d\mathbf{r}'. \tag{9}$$

These interactions lead to a term that is nonlinear in density n and the resulting equations are to be solved iteratively.

Additionally, interactions between protons in the solvent and fixed charges in biomolecules are described as

$$U_{\rm Ion-Fix}(\mathbf{r}) = \sum_{i=1}^{N_a} \frac{q n(\mathbf{r}) Q_i}{\epsilon(\mathbf{r})|\mathbf{r}-\mathbf{r}_i|}. \tag{10}$$

This contribution can be handled by the so called Dirichlet to Neumann mapping approach.[9]

Finally, interactions between protons and other ion species are of the form

$$U_{\rm Ion-Other}(\mathbf{r}) = \sum_{j=1}^{N_c'} \int \frac{q q_j n(\mathbf{r}) n_j'(\mathbf{r}')}{\epsilon(\mathbf{r})|\mathbf{r}-\mathbf{r}'|} d\mathbf{r}'. \tag{11}$$

where the other ionic densities are determined from the continuum Boltzmann distribution in the solvent region with a given profile of electrostatic potential as shown in Eq. (4). Therefore, the electrostatic potential energy functional of protons is

$$\int \left[U_{\rm Ion-Ion}(\mathbf{r}) + U_{\rm Ion-Fix}(\mathbf{r}) + U_{\rm Ion-Other}(\mathbf{r})\right] d\mathbf{r}.$$

Non-electrostatic potential. The electrostatic potential plays a dominant role in the ion channel process. However, non-electrostatic effects are also important to ion conductance efficiency. Sometimes, non-electrostatic effects can even determine the channel selectivity. Non-electrostatic effects physically originate from van der Waals interactions, ion-water dipolar interactions, ion-water cluster formation/dissociation, temperature and entropy effects, etc. For example, one of non-electrostatic effects is an energy barrier to the ion transport due to the change in the solvation environment from the bulk water

to a relatively dry channel pore. However, due to the lack of a comprehensive understanding of the ion behavior in channel region, the modeling of non-electrostatics is less quantitative, compared to the electrostatic modeling. In the Brownian dynamics model and the PNP theory, these non-electrostatic effects are encapsulated in the relaxation time and diffusion coefficients, respectively, which are obtained from experimental data and tuned in a reasonable biological range to predict new results. Here we also set up a reduced model for non-electrostatics potential energy, denoted as $U_{\rm Nonelec}$. Similar to the electrostatics, the $U_{\rm Nonelec}$ is also a functional of the ion density $n(\mathbf{r})$ and includes two contributions: One is the interaction among the target ions themselves, which represents those short range interactions and possible collisions; the other is the interaction between the ion and the surrounding water molecules, which may include the ion-water collisions and dehydration effects. In an analogous structure of energy (9), the former should be a quadratic form while the latter is a linear form like Eq. (10) of the ion density $n(\mathbf{r})$. Based on these considerations, we assume that the non-electrostatic potential energy functional has the following form

$$\int U_{\rm Nonelec}(\mathbf{r})d\mathbf{r} = \int V_{\rm Nonelec}(\mathbf{r})n(\mathbf{r})d\mathbf{r} = \int \left(\alpha k_B T \int n_j^0 d\mathbf{r}' + V_{\rm Ion-sur}(\mathbf{r})\right) n(\mathbf{r})d\mathbf{r} \tag{12}$$

For the first term of Eq. (12), the quadratic form of the density functional is reduced to a linear form by replacing one of the density $n(\mathbf{r})$ by the system reference concentration n_j^0. The reason to do so is that one has to establish the connection of the non-electrostatic potential energy with the total provided ion number. Intuitively, if more ions exist in the system, the possibility of the ion-ion non-electrostatic interaction is higher. The energy resulting from the ion-surrounding interaction is simply modeled as energy $V_{\rm Ion-sur}$, which can be considered as related to the relaxation time of ions. The range o $V_{\rm Ion-sur}$ value is discussed in Section III.E. Here α is a relative weighting parameter for balancing the contribution of two components in the overall $U_{\rm Nonelec}[n(\mathbf{r})]$.

External potentials Since the extracellular and intracellular surroundings can be infinitely large, it is impossible to include them in a detailed description. In the present work, we make appropriate truncation of the surrounding system. As such, the interaction of channel protons with extracellular and intracellular surroundings are described by external potentials $U_{\rm Exter}$. In addition to the truncation effect, the external potentials also describe the experimental conditions such as the effect of given extracellular and intracellular bulk concentrations. We denote channel potential energy functional as

$$\int U_{\rm Exter}d\mathbf{r} = \int V_{\rm Exter}(\mathbf{r})n(\mathbf{r})d\mathbf{r} = \int \left[V_{\rm Extra}(\mathbf{r})n(\mathbf{r}) + V_{\rm Intra}(\mathbf{r})n(\mathbf{r})\right] d\mathbf{r} \tag{13}$$

where $V_{\rm Extra}n(\mathbf{r})$ and $V_{\rm Intra}n(\mathbf{r})$ are extracellular and intracellular positions, respectively. Because much of extracellular and intracellular surrounding is not explicitly described, $V_{\rm Exter}$ must be non-hermitian. This aspect is discussed in Section II.E.

Proton total energy functional. The total proton potential consists of electrostatic, non-electrostatic and external potentials

$$\begin{aligned} U(\mathbf{r}) &= U_{\rm Elec}(\mathbf{r}) + U_{\rm Nonelec}(\mathbf{r}) + U_{\rm Exter} \\ &= \frac{1}{2}\int \frac{q^2 n(\mathbf{r})n(\mathbf{r}')}{\epsilon(\mathbf{r})|\mathbf{r}-\mathbf{r}'|}d\mathbf{r}' + \sum_{i=1}^{N_a}\frac{qn(\mathbf{r})Q_i}{\epsilon(\mathbf{r})|\mathbf{r}-\mathbf{r}_i|} + \sum_{j=1}^{N_c'}\int \frac{qq_j n(\mathbf{r})n_j'(\mathbf{r}')}{\epsilon(\mathbf{r})|\mathbf{r}-\mathbf{r}'|}d\mathbf{r}' \\ &+ V_{\rm Nonelec}(\mathbf{r})n(\mathbf{r}) + V_{\rm Exter}(\mathbf{r})n(\mathbf{r}). \end{aligned} \tag{14}$$

Thus, the total free energy functional of protons includes kinetic and potential contributions

$$G_{\rm Ion}[\Phi, n] = \int \left[\frac{\hbar^2 e^{-(E-E_{\rm Ext})/k_B T}}{2m(\mathbf{r})}|\nabla\Psi_E(\mathbf{r})|^2 dE + U(\mathbf{r})\right] d\mathbf{r}, \tag{15}$$

where each kinetic energy term is weighted by the Boltzmann distribution, which is similar to the treatment in our recent work.[9]

II.C Total free energy functional of the system

To understand the behavior of protons and their interactions, we consider a total free energy functional that includes all significant kinetic and potential energies. Similar energy framework has been developed in our recent work for biomolecular systems and nano-electronic devices.[9,12,54] The total free energy functional of the present system is given by the combination of the electrostatic energy of the system and the quantum mechanical energy of protons. However, it is important to avoid double counting when one constructs the total energy functional.[54] For the present system, it is interesting to note that had the charge sources $qn(\mathbf{r}') + \sum_{i=1}^{N_a} Q_i\delta(\mathbf{r}-\mathbf{r}') + \sum_{j=1}^{N_c'} q_j n_j'(\mathbf{r}')$ been independent of Φ, we would have

$$qn(\mathbf{r})\Phi(\mathbf{r}) = \frac{1}{2}\int \frac{q^2 n(\mathbf{r})n(\mathbf{r}')}{\epsilon(\mathbf{r})|\mathbf{r}-\mathbf{r}'|}d\mathbf{r}' + \sum_{i=1}^{N_a}\frac{qn(\mathbf{r})Q_i}{\epsilon(\mathbf{r})|\mathbf{r}-\mathbf{r}_i|} + \sum_{j=1}^{N_c'}\int \frac{qq_j n(\mathbf{r})n_j'(\mathbf{r}')}{\epsilon(\mathbf{r})|\mathbf{r}-\mathbf{r}'|}d\mathbf{r}' \tag{16}$$

in a homogeneous dielectric medium. Therefore, the charge source for the electrostatic potential also serves the electrostatic potential energy for protons. With this consideration, we propose the total free energy functional

$$\begin{aligned} G_{\rm Total}[\Phi, n] &= \int\left\{\left[\frac{\epsilon(\mathbf{r})}{2}|\nabla\Phi|^2 - \rho(\mathbf{r})\Phi\right]\right. \\ &- \left[\int \frac{\hbar^2 e^{-(E-E_{\rm Ext})/k_BT}}{2m(\mathbf{r})}|\nabla\Psi_E(\mathbf{r})|^2 dE + U_{\rm Nonelec}(\mathbf{r})n(\mathbf{r}) + U_{\rm Exter}(\mathbf{r})n(\mathbf{r})\right. \\ &\left.\left. - \int Ee^{-(E-E_{\rm Ext})/k_BT}|\Psi_E(\mathbf{r})|^2 dE\right]\right\} d\mathbf{r}. \end{aligned} \tag{17}$$

where the total charge sources are given by

$$\rho(\mathbf{r}) = \rho_p(\mathbf{r}) + \rho_f(\mathbf{r}) + \rho'(\mathbf{r}) \tag{18}$$

and the last term in Eq. (17) is the Lagrange multiplier for the energy constraint. The energy functional (17) is a truly multi-physical and multi-scale framework that contains the continuum approximation for solvent and membrane while explicitly takes into account for the channel protein in a discrete fashion. More importantly, it mixes the classical theory and quantum mechanical descriptions in an equal footing.

Note that Eq. (17) is a typical minimization-maximization problem, where the electrostatic free energy is to be minimized while the kinetic energy of protons is to be maximized. Fortunately, this situation does not create a problem as the optimization of the total free energy functional is achieved with two governing equations as described in the next section.

II.D Governing equations

The present system has two unknown functions: the electrostatic potential Φ and the wavefunction Ψ_E. All other functions either are to be explicitly given or depend on Φ and Ψ. The governing equations for Φ and Ψ_E are to be derived from the free energy functional by variational principle via the Euler-Lagrange equation. This multiscale variational framework approach was developed in our recently work.[9,54] It offers successful predictions of the solvation free energies of proteins and small compounds.[12,13]

II.D.1 Generalized Poisson-Boltzmann equations

The total free energy functional given above determines the density distribution and dynamics of protons. The governing equation for electrostatic potential can be derived by the variation of the functional with respect to the potential Φ

$$\frac{\delta G_{\rm Total}[\Phi, n]}{\delta\Phi} \Longrightarrow -\nabla\cdot(\epsilon(\mathbf{r})\nabla\Phi) = \rho(\mathbf{r}), \tag{19}$$

where $\rho(\mathbf{r})$ is defined in Eq. (18). Equation (19) is a generalized Poisson-Boltzmann (GPB) equation describing the electrostatic potential generated from three types of charge sources: the ions of interest, other ions species in the solvent described by the continuum approximation and the fixed point charges

in biomolecules. This equation is not closed because $n(\mathbf{r})$ needs to be evaluated from another governing equation.

A special case of Eq. (19) is also very interesting. Let us assume that all ions in the system are described either by fixed point charges from biomolecules, or by the continuum treatment. Therefore, the system is closed and we arrive at the classical Poisson-Boltzmann equation

$$-\nabla\cdot(\epsilon(\mathbf{r})\nabla\Phi)=\rho_f(\mathbf{r})+\rho_s(\mathbf{r}), \tag{20}$$

where $\rho_s(\mathbf{r})=\sum_{j=1}^{N_c}q_jn_j'(\mathbf{r})$, and N_c is for all ions in the continuum solvent.

II.D.2 Generalized Kohn-Sham equations

In the present multiscale model, the density n of protons in Eq. (19) is governed by generalized Kohn-Sham equations. This set of equations is obtained by the variation of the total free energy functional with respect to wavefunction Ψ_E^*

$$\frac{\delta G_{\rm Total}[\Phi,n]}{\delta\Psi_E^*}\Longrightarrow-\nabla\cdot\frac{\hbar^2}{2m(\mathbf{r})}\nabla\Psi_E(\mathbf{r})+V(\mathbf{r})\Psi_E(\mathbf{r})=E\Psi_E(\mathbf{r}) \tag{21}$$

where

$$V(\mathbf{r})=q\Phi(\mathbf{r})+V_{\rm Nonelec}(\mathbf{r})+V_{\rm Exter}(\mathbf{r})$$

is the effective potential, which includes electrostatic, non-electrostatic and external interactions. The effective potential is discussed in Section II.B.3.

Equation (21) appears to be the conventional Kohn-Sham equation. However, there are some important differences. First, the exchange-correlation potential, which is crucial to electrons, is not presented in Eq. (7). The origin of the exchange-correlation potential is from the Fermi-Dirac distribution, spin and many other unknown effects. In the present theory, we use the non-electrostatic potential to represent many unaccounted effects. We assume the Boltzmann statistics for ions of interest at ambient temperature. Additionally, we define the density as in Eq. (7), instead of the conventional choice for electrons: $n_{\rm electron}(\mathbf{r})=\sum_j|\Psi_j(\mathbf{r})|^2$. This definition is partially due to the Boltzmann statistics and partially due to the spectrum of the present Kohn-Sham operator, which is bounded from below. Technically, the Hamiltonian of the generalized Kohn-Sham equation (21) has not only discrete spectra, but also absolute continuum spectrum. As such, a Boltzmann factor in the density definition is indispensable. Finally, unlike the conventional Kohn-Sham equation, the present generalized Kohn-Sham equation is not a closed one. It is inherently coupled to the generalized Poisson-Boltzmann equation (19). This coupled Kohn-Sham and Poisson-Boltzmann system endows us the flexibility to deal with complex multiphysics in a multiscale fashion — the quantum dynamics in continuum.

II.E Proton density operator for the non-hermitian Hamiltonian

As mentioned earlier, the external potential has a non-hermitian component to describe the interaction with truncated extracellular and intracellular surroundings. Let us explicitly separate the anti-hermitian (or skew hermitian) components

$$V_{\rm Extra}=V_{\rm Extra}^h+V_{\rm Extra}^{ah},\quad V_{\rm Intra}=V_{\rm Intra}^h+V_{\rm Intra}^{ah}, \tag{22}$$

where

$$V_\alpha^h=\frac{1}{2}(V_\alpha+V_\alpha^\dagger),\quad V_\alpha^{ah}=\frac{1}{2}(V_\alpha-V_\alpha^\dagger),\quad \alpha={\rm Extra},\ {\rm Intra}. \tag{23}$$

The non-hermitian parts of the external potentials describe the relaxation effect or spectral line shape broadening due to the interaction with the surroundings. Accordingly, we split the Hamiltonian as

$$H=H^h+V^{ah}=H^h+V_{\rm Extra}^{ah}+V_{\rm Intra}^{ah}. \tag{24}$$

We first note that the density of protons can be further given by

$$n_H=\int e^{-(E-E_{\rm Ext})/k_BT}\delta(E-H)dE. \tag{25}$$

In this work, we define the spectral operator $\delta(E-H)$ as

$$\delta(E-H)=\frac{i}{2\pi}\lim_{\varepsilon\to 0}\lim_{\|V^{ah}\|\to 0}\left[\frac{1}{E-(H-i\varepsilon)}-\frac{1}{E-(H-i\varepsilon)^{\dagger}}\right] \tag{26}$$

We therefore approximate the proton density operator by

$$n_H=\frac{i}{2\pi}\int e^{-(E-E_{\rm Ext})/k_BT}\left[G(E)-G^{\dagger}(E)\right]dE, \tag{27}$$

where G is the Green's function (operator)

$$G(E)=(E-H)^{-1}. \tag{28}$$

We therefore arrive at a useful expression for the proton density

$$\begin{aligned} n_H &= \frac{i}{\pi}\int e^{-(E-E_{\rm Ext})/k_BT}\left[\sum_{\alpha}G(E)V_{\alpha}^{ah}G^{\dagger}(E)\right]dE & (29)\\ &= \frac{i}{\pi}\sum_{\alpha}\int e^{-(E-E_{\alpha})/k_BT}G(E)V_{\alpha}^{ah}G^{\dagger}(E)dE, \quad \alpha=\text{Extra, Intra}, & (30)\end{aligned}$$

where $E_{\rm Extra}$ and $E_{\rm Intra}$ are the external electrical field energies at extracellular and intracellular electrodes, respectively. Note that $E_{\rm Ext}$ behaves like an operator such that its value is chosen according to the nearest external interaction. Equation (30) provides an appropriate expression for computing the total proton density.

II.F Proton transport

Typically, external electrical field is applied as the difference of electrical potentials, $(E_{\rm Extra}/q-E_{\rm Intra}/q)$. The experimental measurements are given as the current and voltage curve, or the so called I-V curve. Therefore, a major goal of our theoretical model is to provide predictions of the current under different external voltages. The current in the standard quantum mechanics is given by

$$\begin{aligned} I &= q{\rm Tr}\frac{1}{2}\left(n_Hv^{\dagger}+vn_H\right) & (31)\\ &= q\int\int\frac{\hbar}{2mi}\left[\Psi_E^*(\mathbf{r})\nabla\Psi_E(\mathbf{r})-\Psi_E(\mathbf{r})\nabla\Psi_E^*(\mathbf{r})\right]e^{-(E-E_{\rm Ext})/k_BT}d\mathbf{r}dE, & (32)\end{aligned}$$

where ${\rm Tr}$ is the trace operation and $\frac{1}{2}\left(n_Hv^{\dagger}+vn_H\right)$ is the symmetrized current operator with v being the velocity vector. Equation (32) requires the evaluation of the full scattering wavefunction $\Psi_E(\mathbf{r})$. The spatial derivative can be carried out at a location consistent with the specific feature of the external electrical field $E_{\rm Ext}$.

An alternative current expression can be given by examining the transition rates due to the anti-hermitian parts of the external interaction potential. Let us evaluate the transition rate according to the interaction potential $V_{\rm Extra}^{ah}$

$$\begin{aligned} I &= q\frac{1}{i\hbar}{\rm Tr}\frac{1}{2}\left[n_H\left(V_{\rm Extra}^{ah}\right)^{\dagger}+V_{\rm Extra}^{ah}n_H\right] & (33)\\ &= \frac{q}{\hbar}{\rm Tr}\left\{\int e^{-(E-E_{\rm Ext})/k_BT}\sum_{\alpha}G(E)V_{\alpha}^{ah}G^{\dagger}(E)\left(V_{\rm Extra}^{ah}\right)^{\dagger}dE\right.\\ &+ \left.\int V_{\rm Extra}^{ah}e^{-(E-E_{\rm Ext})/k_BT}\sum_{\alpha}G(E)V_{\alpha}^{ah}G^{\dagger}(E)dE\right\} & (34)\end{aligned}$$

Now we need to make a decision for $E_{\rm Ext}$ because each term involves two interaction potentials. In this work, we systematically choose $E_{\rm Ext}$ according to the nearest external interaction

$$\begin{aligned} I &= \frac{q}{h}\mathrm{Tr}\left\{\int e^{-(E-E_\alpha)/k_BT}\sum_\alpha G(E)V_\alpha^{ah}G^\dagger(E)\left(V_{\rm Extra}^{ah}\right)^\dagger dE \right. \\ &+ \left. \int V_{\rm Extra}^{ah}e^{-(E-E_{\rm Extra})/k_BT}\sum_\alpha G(E)V_\alpha^{ah}G^\dagger(E)dE\right\} \qquad (35) \\ &= \frac{q}{h}\mathrm{Tr}\int G(E)V_{\rm Intra}^{ah}G^\dagger(E)V_{\rm Extra}^{ah}\left[e^{-(E-E_{\rm Extra})/k_BT}-e^{-(E-E_{\rm Intra})/k_BT}\right]dE \qquad (36) \end{aligned}$$

Similarly, we obtain a current expression by using the interaction potential $V_{\rm Intra}^{ah}$

$$\begin{aligned} I &= q\frac{1}{i\hbar}\mathrm{Tr}\frac{1}{2}\left[n_H\left(V_{\rm Intra}^{ah}\right)^\dagger + V_{\rm Intra}^{ah}n_H\right] \\ &= \frac{q}{h}\mathrm{Tr}\int G(E)V_{\rm Extra}^{ah}G^\dagger(E)V_{\rm Intra}^{ah}\left[e^{-(E-E_{\rm Intra})/k_BT}-e^{-(E-E_{\rm Extra})/k_BT}\right]dE \qquad (37) \end{aligned}$$

Equations (36) and/or (37) can be used for current evaluations under different external electrical field strengths and concentrations.

III Computational algorithms

The implementation of the theoretical model described in Section II.D involves a number of computational issues. The present section is devoted to the computational implementation of our quantum dynamics in continuum model.

III.A Proton density structure and transport

Proton density structure concerns the solution of the generalized Kohn-Sham equation whereas the proton transport offers the current-voltage curves, which are to be compared with experimental measurement. This subsection describes the solution strategy of the generalized Kohn-Sham equation and theoretical prediction of experimental data.

III.A.1 The solution of the generalized Kokn-Sham equation

Typically, solving the full-scale Kohn-Sham equation can be a major obstacle in the simulation. Due to the fact that biological characteristics for each subdomain of the ion channel system are quite different and the Kohn-Sham operator will have distinct properties correspondingly. In this subsection, we make use of various decomposition schemes to reduce the computational complexity in solving Eq. (21).

Motions of quantum particles in the present system can be generally classified into three categories: scattering along transport directions, confined motion and free motion. The channel pore direction (i.e., the z direction) is designated as the transport direction, in which protons cross the transmembrane protein or scatter back to the solvent. Along the z direction, the Kohn-Sham operator has an absolutely continuous spectrum. In the $x-y$ directions, the Kohn-Sham equation possesses different behaviors. In the extracellular and intracellular regions where the solvent domains are sufficiently large, proton motions are essentially unconfined in the $x-y$ directions. They undergo intensive electrostatic and non-electrostatic interactions although the system can be regarded as near the equilibrium. The associated Kohn-Sham operator for protons also has an absolutely continuous spectrum. In contrast, in channel pore region, the protons are confined in $x-y$ plane by the channel wall. In the confined plane, the Kohn-Sham operator is essentially compact and has a discrete spectrum. For two different regions, formulations and corresponding treatments of the proton density are different.

The proton density structure in the channel pore is crucial to the proton transport. Whereas, the behavior of protons in the bath is relatively less important. Therefore, as a good approximation, we can truncate the computational domain in the bath regions. Consequently, the Kohn-Sham operator becomes compact for all $x-y$ directions and has discrete eigenvalues. As a good approximation for many ion channels, we split the total wavefunction $\Psi_E(\mathbf{r})$ as

$$\Psi_E(\mathbf{r}) = \psi^j(x,y;z)\psi_k^j(z) \qquad (38)$$

where $\psi^j(x,y;z)$ is the j-th eigen-mode in the confined directions at a specific location z, and $\psi_k^j(z)$ is the wavefunction along the transport direction, with transport wave number k. Under this circumstance, it is convenience to relabel the total energy E as E_k^j, where j and k are related to the energies for confined and transport directions, respectively. If the mode-mode interaction along the confined direction is neglected, it is easy to verify that ψ^j and ψ_k^j satisfy the following decomposed Kohn-Sham equations,

$$\left[-\frac{\hbar^2}{2}\left(\frac{\partial}{\partial x}\frac{1}{m_x}\frac{\partial}{\partial x}+\frac{\partial}{\partial y}\frac{1}{m_y}\frac{\partial}{\partial y}\right)+V(x,y;z)\right]\psi^j(x,y;z_0)=U^j(z)\psi^j(x,y;z) \tag{39}$$

$$\psi^j(x,y;z)=0 \quad \text{on} \quad \partial\Omega_D(z);$$

$$\left[-\frac{\hbar^2}{2}\frac{\partial}{\partial z}\frac{1}{m_z}\frac{\partial}{\partial z}+U^j(z)\right]\psi_k^j(z)=E_k^j\psi_k^j(z), \quad j=1,2,\cdots, \tag{40}$$

where $V(x,y;z)$ is the restriction of the potential operator $V(x,y,z)$ at position z, $U^j(z)$ is the jth eigenvalue of the 2D problem at position z, and $\psi^j(x,y;z)$ is the corresponding eigenfunction. Here $\psi_k^j(z)$ is the scattering wavefunction associated with the scattering potential $U^j(z)$. Here $\partial\Omega_D(z)$ is the boundary for the cross section at z. The transport equation (40) can be solved as a scattering problem. Finally the proton density (7) can be modified as

$$\begin{aligned} n(\mathbf{r}) &= \sum_j \int |\psi^j(x,y;z)|^2 |\psi_k^j(z)|^2 e^{-(E_k^j-E_{\rm Ext})/k_BT} dE_k^j \\ &\doteq \sum_j |\psi^j(x,y;z)|^2 n_{\rm scat}^j(z). \end{aligned} \tag{41}$$

Equation (41) only gives the symbolic proton density structures for an unspecified $E_{\rm Ext}$. More detailed consideration of $E_{\rm Ext}$ requires the further treatment of the scattering boundary conditions as shown in Sections II.E and II.F. However, the 2D wavefunction $|\psi^j(x,y;z)|^2$ in Eq. (41) can be evaluated from the Kohn-Sham equation (39). The solution to this equation is quite standard — it is just the eigenvalue problem of an equation of elliptic type. While to solve the transport problem, as indicated in the theory, one needs to find appropriate expressions of the non-hermitian external operators. The corresponding computational aspects are presented in the next subsection.

III.A.2 Boundary treatment of the transport calculation

Although the quantum confinement Eq. (39) only happens in finite channel region, the transport problem Eq. (40) is associated with infinitely large surroundings, in principle. Since the same procedure is used to solve Eq. (40) for different j, let us drop the j label

$$\left(-\frac{\hbar^2}{2}\frac{\partial}{\partial z}\frac{1}{m_z}\frac{\partial}{\partial z}+U\right)\psi_k(z)=E\psi_k(z), \quad z\in(-\infty,\infty), \tag{42}$$

where $-\frac{\hbar^2}{2}\frac{\partial}{\partial z}\frac{1}{m_z}\frac{\partial}{\partial z}+U$ is the scattering Hamiltonian and E is the scattering energy. In practical computations, the extracellular and intracellular surroundings have to be truncated. Suppose $[z_1,z_2]$ is the finite transport interval of interest and the regions $(-\infty,z_1)$ and (z_2,∞) are assumed as infinitely long extracellular and intracellular environments. We assume that in regions $(-\infty,z_1)$ and (z_2,∞), the interaction potential U is independent of position due to the spatial average of homogenization type over the large scale. Consequently, Eq. (42) admits planewave solutions asymptotically. For instance, if one considers the wavefunctions $\psi_k(z)$ in the extracellular environment, it has the following form

$$\begin{array}{ll} \psi_k(z)=e^{ikz}+r_me^{-ikz} & \text{if } z\in(-\infty,z_1) \\ \psi_k(z)=t_me^{ikz} & \text{if } z\in(z_2,\infty) \end{array} \tag{43}$$

where r_m and t_m are reflection and transmission coefficients, respectively. Given the specific formulation of the wavefunction in the extracellular bath, Eq. (43) can be employed as boundary conditions of Eq. (42) to obtain the proton density originated from the extracellular part. Similar boundary conditions for the intracellular part can be derived in the same fashion.

Suppose that the interval $[z_1, z_2]$ is discretized as $z_1, z_2, ..., z_N$, where N is the total number of grid points and the grid size is denoted as $\Delta z = (z_2 - z_1)/N$. For simplicity, let $t = \frac{\hbar^2}{2m_z(\Delta z)^2}$, then for interior points $z_i, (i = 2, ..., N-1)$, the discretization of Eq. (42) is quite standard by the finite difference method

$$-t\psi_{i-1} + (2t + U_i - E)\psi_i - t\psi_{i+1} = 0 \tag{44}$$

where ψ_i represents the numerical solution of $\psi_k(z_i)$ and U_i is for $U(z_i)$. For the discretization at boundary point z_1, we first define a fictitious function value of $\psi(z)$ on z_0, the point ahead of z_1 as ψ_0, then the discretization at z_1 is

$$-t\psi_0 + (2t + U_i - E)\psi_1 - t\psi_2 = 0. \tag{45}$$

Now one needs to determine the fictitious value ψ_0 in terms of $\psi_i, (i = 1, 2, ..., N)$. From the boundary condition (43), we have

$$\begin{array}{l} \psi_0 = e^{ik_0 z_0} + r_m e^{-ik_0 z_0} \\ \psi_1 = e^{ik_1 z_1} + r_m e^{-ik_1 z_1}. \end{array} \tag{46}$$

In fact, we have $k_0 = k_1$ since the free motion of the wave in the asymptotic regions. We can denote k_0 and k_1 by k_1 with $\frac{(\hbar k_1)^2}{2m_z} = E - U_1$. By this notation, we have

$$\begin{array}{rcl} \psi_0 - \psi_1 e^{ik_1\Delta z} & = & e^{ik_1 z_0} - e^{ik_1(z_1+\Delta z)} \\ & = & e^{ik_1(z_1-\Delta z)} - e^{ik_1(z_1+\Delta z)}. \end{array} \tag{47}$$

Inserting Eq. (47) into Eq. (45), one yields

$$-t\psi_1 e^{ik_1\Delta z} + (2t + U_1 - E)\psi_1 - t\psi_2 = -2ti\sin(k_1\Delta z)e^{ik_1 z_1}. \tag{48}$$

Applying the same strategy for ψ_N and fictitious function value ψ_{N+1}, we have

$$\psi_{N+1} - \psi_N e^{ik_N\Delta z} = t_m e^{ik_N z_{N+1}} - t_m e^{ik_N z_N} e^{ik_N\Delta z} = 0, \tag{49}$$

where $\frac{(\hbar k_N)^2}{2m_z} = E - U_N$ and further

$$-t\psi_{N-1} + (2t + U_N - E)\psi_N - t\psi_N e^{ik_N\Delta z} = 0. \tag{50}$$

Follow the same boundary treatment for the intracellular environment, the whole system is discretized in vector and matrix forms as the following

$$\mathbf{G}^{-1}\mathbf{\Psi}_{\text{Extra}} = (\mathbf{H^s} - E\mathbf{I})\mathbf{\Psi} = \mathbf{b}_{\text{Extra}} \tag{51}$$

where $\mathbf{\Psi}_{\text{Extra}} = (\psi_1, \psi_2, ..., \psi_N)^T$, $\mathbf{I}$ is the identity matrix of dimension $N \times N$ and

$$\mathbf{H^s} = \begin{pmatrix} 2t + U_1 - te^{ik_1\Delta z} & -t & \dots & \dots & 0 \\ -t & 2t + U_2 & -t & \dots & 0 \\ \vdots & \vdots & \vdots & \ddots & \vdots \\ 0 & \dots & \dots & -t & 2t + U_N - te^{ik_N\Delta z} \end{pmatrix}_{N\times N}. \tag{52}$$

Here $\mathbf{b}_{\text{Extra}}$ is the source term for the incoming waves from the extracellular surroundings

$$\mathbf{b}_{\text{Extra}} = (2ti\sin(k_1\Delta z)e^{ik_1 z_1}, 0, \dots, 0)^T. \tag{53}$$

The wavefunction $\mathbf{\Psi}_{\text{Extra}}$ can be written as

$$\mathbf{\Psi}_{\text{Extra}} = \mathbf{G}\mathbf{b}_{\text{Extra}}. \tag{54}$$

Let $\mathbf{\Psi}^{\dagger}_{\rm Extra}$ be the complex conjugate of $\mathbf{\Psi}_{\rm Extra}$. We have

$$\mathbf{\Psi}_{\rm Extra}{\mathbf{\Psi}_{\rm Extra}}^{\dagger} = \mathbf{G}\mathbf{b}_{\rm Extra}\mathbf{b}^{\dagger}_{\rm Extra}\mathbf{G}^{\dagger} = \mathbf{G}\begin{pmatrix} [2t\sin(k_1\Delta z)]^2 & 0 & \dots & \dots & 0 \\ 0 & \dots & \dots & \dots & 0 \\ \vdots & \vdots & \vdots & \ddots & \vdots \\ 0 & \dots & \dots & \dots & 0 \end{pmatrix}\mathbf{G}^{\dagger}. \tag{55}$$

Similar derivation can be carried out for the wavefunction $\Psi_{\rm Intra}$ related to intracellular surroundings,

$$\mathbf{\Psi}_{\rm Intra}{\mathbf{\Psi}_{\rm Intra}}^{\dagger} = \mathbf{G}\mathbf{b}_{\rm Intra}\mathbf{b}^{\dagger}_{\rm Intra}\mathbf{G}^{\dagger} = \mathbf{G}\begin{pmatrix} 0 & 0 & \dots & \dots & 0 \\ 0 & \dots & \dots & \dots & 0 \\ \vdots & \vdots & \vdots & \ddots & \vdots \\ 0 & \dots & \dots & \dots & [2t\sin(k_N\Delta z)]^2 \end{pmatrix}\mathbf{G}^{\dagger}. \tag{56}$$

Therefore, the total density matrix is

$$\mathbf{D} = \frac{1}{2\pi}\int\left[\sum_{\alpha} e^{-(E-E_\alpha)/k_BT}\mathbf{G}\mathbf{b}_\alpha{\mathbf{b}_\alpha}^{\dagger}\mathbf{G}^{\dagger}\right]dk, \quad \alpha = \text{Extra, Intra.} \tag{57}$$

Use the relation

$$dE = d\frac{(\hbar k)^2}{2m} + 0 = \frac{\hbar^2 k}{m}dk \tag{58}$$

to change the above integral into that with respect to energy E, and use the simple limit $\sin(k\Delta z)/(k\Delta z) \to 1$ as $\Delta z \to 0$, the above integral can be easily revised as

$$\mathbf{D} = \frac{i}{\pi\Delta z}\int\left[\sum_{\alpha} e^{-(E-E_\alpha)}\mathbf{G}V^{ah}_{\alpha}\mathbf{G}^{\dagger}\right]dE, \quad \alpha = \text{Extra, Intra,} \tag{59}$$

where

$$V^{ah}_{\rm Extra} = \begin{pmatrix} -it\sin(k_1\Delta z) & 0 & \dots & \dots & 0 \\ 0 & \dots & \dots & \dots & 0 \\ \vdots & \vdots & \vdots & \ddots & \vdots \\ 0 & \dots & \dots & \dots & 0 \end{pmatrix} \tag{60}$$

and

$$V^{ah}_{\rm Intra} = \begin{pmatrix} 0 & 0 & \dots & \dots & 0 \\ 0 & \dots & \dots & \dots & 0 \\ \vdots & \vdots & \vdots & \ddots & \vdots \\ 0 & \dots & \dots & \dots & -it\sin(k_N\Delta z) \end{pmatrix}. \tag{61}$$

It is clear that $V_{\rm Extra}$ and $V_{\rm Intra}$ are the non-hermitian components in the external potential Eq. (22) that are introduced to truncate the surroundings. Since V^{ah}_{α} is solely nonzero for one entry in the matrix and this fact is independent of the discretization, it is easy to verify that $\lim_{\Delta z\to 0}||V^{ah}_{\alpha}|| = 0$, as required in Eq. (26).

Obviously, Eq. (59) is actually the discretization form of Eq. (30). Finally, the scattering number density is calculated as

$$n_{\rm scat}(z) = \text{diag}(\mathbf{D}). \tag{62}$$

III.B Dirichlet-to-Neumann mapping for the generalize PB equation

Considering Eq. (4) and expression (19), the generalized Poisson-Boltzmann equation is

$$-\nabla\cdot(\epsilon(\mathbf{r})\nabla\Phi) = qn(\mathbf{r}) + \sum_{i=1}^{N_a} Q_i\delta(\mathbf{r}-\mathbf{r}_i) + \sum_{j=1}^{N_c'} q_j n_j^0 e^{-\frac{q_j(\Phi-V_{\rm Ext})}{k_BT}} \tag{63}$$

Recall the fact that the electrostatic potential $\Phi(\mathbf{r})$ is defined throughout the domain Ω, which is inhomogeneous with respect to the dielectric constant $\epsilon(\mathbf{r})$. Therefore, we need to physically impose the continuity matching conditions at the interface Γ of two adjunctive subregions. The continuity matching conditions are given as

$$[\Phi]|_\Gamma = \Phi^+(\mathbf{r}) - \Phi^-(\mathbf{r}) = 0, \tag{64}$$

$$[\epsilon\nabla\Phi\cdot\vec{\mathbf{n}}]|_\Gamma = \epsilon^+\nabla\Phi^+(\mathbf{r})\cdot\vec{\mathbf{n}} - \epsilon^-\nabla\Phi^-(\mathbf{r})\cdot\vec{\mathbf{n}} = 0 \tag{65}$$

where superscripts "$^+$" and "$^-$" represent the limiting values of a certain function at two sides of interface Γ, and $\vec{\mathbf{n}}$ is the unit outward normal direction of Γ. Equation (65) guarantees the continuities of the potential function and its flux.

Theoretically, Eq. (63) admits the boundary condition $\Phi(\infty) = 0$ at the infinity. However, in practical computation, a finite domain is used and appropriate boundary conditions need to be imposed at the domain boundary $\partial\Omega$. In our studies, the channel protein and the associated membrane are embedded in a rectangular cuboid with appropriate sizes. It is very nature to apply the Dirichlet boundary conditions along the electrode portions of the rectangular cuboid boundary, while for the remainder of the boundary, we apply the Neumann boundary condition (i.e., the zero normal electric filed conditions).

Physically, the generalized Poisson-Boltzmann equation (63) has two types of charge source terms, i.e., the fixed charges given by the delta functions, and the unsteady charges. Therefore, it is wise to treat these source terms separately such that when we keep updating the unsteady source term, we just need to compute the effect of the fixed charge source term once. Mathematically, the solution of Eq. (63) has a singular part due to the delta function (i.e., fixed charges) which may cause computational problems. Thus, we should treat the regular part and the singular part of the solution differently[27]

$$\Phi = \bar{\Phi} + \tilde{\Phi} \tag{66}$$

where $\bar{\Phi}$ and $\tilde{\Phi}$ denote the singular part and regular part of Φ, respectively. More specifically, $\bar{\Phi}$ should correspond to the singular delta function term and vanish outside the protein and membrane domain Ω_m, while $\tilde{\Phi}$ is defined in the whole domain. By this consideration, we split $\bar{\Phi}(\mathbf{r})$ as

$$\bar{\Phi}(\mathbf{r}) = \Phi^*(\mathbf{r}) + \Phi^0(\mathbf{r}) \tag{67}$$

where

$$\Phi^*(\mathbf{r}) = \sum_{i=1}^{N_a} \frac{Q_i}{\epsilon_m|\mathbf{r}-\mathbf{r}_i|} \tag{68}$$

represents the Coulomb's potential from the protein fixed charges. Since $\bar{\Phi}(\mathbf{r})$ is required to vanish outside the Ω_m as well as the boundary $\partial\Omega_m$, the $\Phi^*(\mathbf{r})$ should be corrected by $\Phi^0(\mathbf{r})$, which is a harmonic function on Ω_m and

$$\Phi^0(\mathbf{r}) = -\Phi^*(\mathbf{r}), \quad \forall\mathbf{r}\in\partial\Omega_m. \tag{69}$$

For the regular part $\tilde{\Phi}$, we can take the advantage of the fact that n_j^0 is zero in Ω_m, and have the following equation and interface jump conditions:

$$-\nabla\cdot\left(\epsilon(\mathbf{r})\nabla\tilde{\Phi}\right) - \sum_{j=1}^{N_c'} q_j n_j^0 e^{-\frac{q_j(\tilde{\Phi}-V_{\rm Ext})}{k_BT}} = qn(\mathbf{r}) \tag{70}$$

$$[\tilde{\Phi}]_\Gamma = 0 \tag{71}$$

$$[\epsilon\nabla\tilde{\Phi}\cdot\vec{\mathbf{n}}]|_\Gamma = -[\epsilon\bar{\Phi}\cdot\vec{\mathbf{n}}]|_\Gamma \tag{72}$$

Through Eqs. (66) to (70), the electrostatic potential Φ is decomposed into a singular part and a regular part. It should be noted that it is $\tilde{\Phi}$ that is coupled to the Kohn-Sham equation since $\bar{\Phi}$ is solely nonzero in the protein and membrane region. The effect of the fixed charges is actually first mapped on the $\partial\Omega_m$ in a Dirichlet sense (Eq. (69)) and reflected into the solvent region in a Neumann manner (Eq. (72)) at the solvent-protein interface Γ. This Dirichlet-to-Neumann mapping (DNM) analytically takes care of the Dirac delta functions and is successfully employed in various applications.[9,27] The trade-off of this treatment is that one has to solve an elliptic equation (70) with non-homogeneous interface jump conditions.

Traditional finite difference or finite element methods fail to come up with high-order accuracy and convergence in solving Eq. (70) due to geometric singularities in the molecular surface[47] and the need to enforce the interface conditions (71) and (72). The matched interface and boundary (MIB) method has been developed for elliptic equations with complex interfaces, geometric singularity, and singular charges.[8,27,55,56,58,59] It offers second-order accuracy and convergence in solving the Poisson-Boltzmann equation with biomolecular context.[8,27,56,58] Therefore, the combination of DNM and MIB provides a robust and efficient solution to the generalized PB equation with second-order accuracy and convergence, even for complex channel protein geometries.

III.C The self-consistent iteration

In this section we analyze the self-consistent iteration between the generalized PB equation and the Kohn-Sham equation. To focus on the essential idea, Eq. (70) is symbolically written as

$$L\tilde{\Phi} + F(\tilde{\Phi}) = \rho_p, \tag{73}$$

where $\tilde{\Phi}$ and ρ_p represent the electrostatic potential energy and proton density, L represents the linear part of the GPB equation while the $F(\tilde{\Phi})$ is the nonlinear part. Simply substituting the quantity ρ_p into Eq. (73) does not offer a clue about the iteration convergence analysis and efficiency. The Gummel iteration[21] proposed in semiconductor device applications was verified practically that it works well for a similar self-consistent iteration problem. The idea of the Gummel iteration is described below.

The proton density ρ_p and the electrostatics potential $\tilde{\Phi}$ are assumed to have the following intrinsic connection

$$\rho_p(\mathbf{r}) = \mathscr{F}(\tilde{\Phi}(\mathbf{r}), E_{\rm Ext}), \tag{74}$$

where $\mathscr{F}(\tilde{\Phi}, E_{\rm Ext}) = qn_0 e^{-(q\tilde{\Phi}-E_{\rm Ext})/k_BT}$ is the Boltzmann function and n_0 is the reference number density of the protons. Equation (74) represents the relation between the electrostatic potential and the particle density in the equilibrium state. However, the relation does not hold any more at non-equilibrium. Nevertheless, we can extend $E_{\rm Ext}$ to a function defined over the entire domain $E_{\rm Ext}(\mathbf{r})$ such that $\rho_p(\mathbf{r}) = \mathscr{F}(\tilde{\Phi}(\mathbf{r}), E_{\rm Ext}(\mathbf{r}))$. The intermediate values of $E_{\rm Ext}(\mathbf{r})$ can be easily found once ρ_p and $\tilde{\Phi}(\mathbf{r})$ are available. Based on this argument, Eq. (73) is written as a new nonlinear equation

$$L\tilde{\Phi} + F(\tilde{\Phi}) = \mathscr{F}(\tilde{\Phi}, E_{\rm Ext}). \tag{75}$$

We need to linearize Eq. (75) appropriately. Note that $\mathscr{F}'(\tilde{\Phi}, E_{\rm Ext}) = -\frac{q}{k_BT}\mathscr{F}(\tilde{\Phi}, E_{\rm Ext}) = -\frac{q}{k_BT}\rho_p$, with $\mathscr{F}'(\tilde{\Phi}, E_{\rm Ext})$ being the Fréchet derivatives of $\mathscr{F}$ with respect to $\tilde{\Phi}$. Similarly, $F'(\tilde{\Phi})$ can be evaluated.

Suppose $\tilde{\Phi}^l$, $E^l_{\rm Ext}$ and ρ^l_p are the values of $\tilde{\Phi}$, $E_{\rm Ext}$ and ρ_p at lth step iteration, then the Newton's method for solving Eq. (75) is naturally reduced to the Gummel iteration:

$$\left(L + F'(\tilde{\Phi}^l) + \frac{q}{k_BT}\rho^l_p\right)\Delta\tilde{\Phi}^l = \rho^l_p - L\tilde{\Phi}^l - F(\tilde{\Phi}^l) \tag{76}$$

where we update $\tilde{\Phi}^{l+1}$ as $\tilde{\Phi}^{l+1} = \tilde{\Phi}^l + \lambda\Delta\tilde{\Phi}^l$ and $0 < \lambda \leq 1$ is chosen through a line search to guarantee

$$||L\tilde{\Phi}^{l+1} + F(\tilde{\Phi}^{l+1}) - \frac{q}{k_BT}\rho^{l+1}_p|| < ||L\tilde{\Phi}^l + F(\tilde{\Phi}^l) - \frac{q}{k_BT}\rho^l_p||. \tag{77}$$

Once $\tilde{\Phi}^{l+1}$ and ρ^{l+1}_p is obtained, $E^{l+1}_{\rm Ext}$ can be modified, and whole iteration can continue till the convergence is achieved. It is worthwhile to point out that in order to improve numerical efficiency, Eq. (76)

can be solved by applying various inexact Newton's methods. There is plenty of literature about the convergence order discussion so it is necessary for us to generalize the Gummel iteration to the Newton's method.

Another technique to enhance the self-consistent convergence is the relaxation method.[9] If we define the K_s, U_s and N_s as the spaces which the external potential $E_{\mathrm{Ext}}(\mathbf{r})$, electrostatics $\tilde{\Phi}(\mathbf{r})$ and proton charge density $\rho(\mathbf{r})$ belong to, respectively. For the whole iteration of the generalized Poisson-Boltzmann Kohn-Sham system, it can be interpreted as the application of the fixed point map $\mathscr{T}$ on any of the above spaces, say $\mathscr{T} : U_s \to U_s$ for the electrostatics

$$\tilde{\Phi}(\mathbf{r}) = \mathscr{T}(\tilde{\Phi}(\mathbf{r})). \tag{78}$$

To characterize the details of the map $\mathscr{T}$, we denote the operator $\mathscr{G} : U_s \to N_s$, which indicates the process of using the Kohn-Sham equation to solve for proton charge density based on the electrostatic potential. Such a process is followed by $\mathscr{F}^{-1} : N_s \to K_s$, which updates $E_{\mathrm{Ext}}(\mathbf{r})$ by $\rho_p(\mathbf{r})$ and $\tilde{\Phi}(\mathbf{r})$. Finally $\mathscr{L} : K_s \to U_s$ represents solving the nonlinear GPB equation. The combination of all the above operations yields the definition of the operator $\mathscr{T}$, which shows the outer iteration

$$\mathscr{T} := \mathscr{L} \circ \mathscr{F}^{-1} \circ \mathscr{G} \tag{79}$$

and

$$\tilde{\Phi}^{l+1} = \mathscr{L} \circ \mathscr{F}^{-1} \circ \mathscr{G}(\tilde{\Phi}^{l}). \tag{80}$$

The relaxation scheme converts Eq. (80) into the steady-state problem of an ordinary differential equation (ODE)

$$\frac{\partial \tilde{\Phi}}{\partial t} = \mathscr{L} \circ \mathscr{F}^{-1} \circ \mathscr{G}(\tilde{\Phi}) - \tilde{\Phi}. \tag{81}$$

Therefore many ODE related techniques such as the Runge-Kutta method can be used to improve the convergence properties. One simple treatment is the discretization of Eq. (81) as

$$\frac{\tilde{\Phi}^{l+1} - \tilde{\Phi}^{l}}{\beta} = \mathscr{L} \circ \mathscr{F}^{-1} \circ \mathscr{G}(\tilde{\Phi}^{n}) - \tilde{\Phi}^{n}, \tag{82}$$

which leads to a self-consistent iteration with a relaxation factor β[9,12]

$$\begin{aligned} \tilde{\Phi}^{\star} &= \mathscr{L} \circ \mathscr{F}^{-1} \circ \mathscr{G}(\tilde{\Phi}^{n}) \\ \tilde{\Phi}^{n+1} &= \beta \tilde{\Phi}^{\star} + (1-\beta)\tilde{\Phi}^{n}. \end{aligned} \tag{83}$$

The traditionally used outer loop iteration actually is the special case of Eq. (83) with $\beta = 1$. By carefully choosing the relax factor β, one can reach the steady state (fix point) by self-consistent iterations.

III.D The work flow of the self-consistent iteration

In previous sections algorithms and related mathematical treatments for solving the GPB equation and the Kohn-Sham equation individually are introduced. Here we assemble all the components together and give a main work flow for the numerical simulation of these coupled equations.

- **Step 0.** Preparation. All the necessary preparations for the whole loop are accomplished in this step, which include:
  - 1. The channel protein of interest is downloaded from the Protein Data Bank. The partial charges, positions, radii of all atoms as well as molecular surfaces are determined by CHARMM force field[36] and related software packages, such as PDB2PQR, see Section IV for detail. The prepared channel structure and surface are then embedded in a proper computational domain.
  - 2. Use Eqs. (68) and (69) to solve for $\bar{\Phi}$, then the quantity in Eq. (72) is obtained. Implement the DNM and the MIB schemes to discretize the Laplace operator as matrix L.

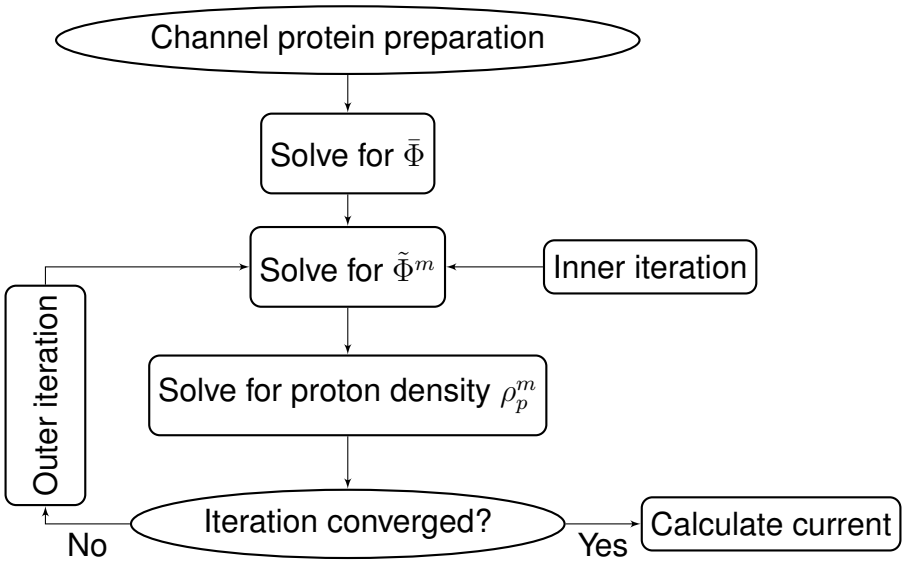

Figure 2: Work flow of the overall self-consistent iteration.

- **Step 1.** Solving the generalized PB equations (70) and (72). Given ρ_p^m (taken an initial guess if $m = 0$), use the inexact Newton's method, Eq. (76) and Eq. (77) to obtain $\tilde{\Phi}^m$. Note that the index l in Eq. (76) is for the Newton's method or inner iteration and the index m is for the outer or whole self-consistent iteration loop.
- **Step 2.** Solving the Kohn-Sham equation. The solution of the Kohn-Sham equation consists of two parts, the eigenvalue problem and the scattering problem with the evaluated electrostatic potential energy operator $U = q\tilde{\Phi}^m$.
  - 1. Solving the eigenvalue problem Eq. (39).
  - 2. Solving the transport problem Eq. (40).
  - 3. Assembling the total charge density n^{m+1} by Eqs. (41) and (62).
- **Step 3.** Convergence check. Go to Step 1 to obtain $\tilde{\Phi}^{m+1}$, if $||\tilde{\Phi}^{m+1} - \tilde{\Phi}^m|| < \varepsilon_1$ and $||\rho_p^{m+1} - \rho_p^m|| < \varepsilon_2$, where ε_1 and ε_2 are predefined error tolerances, then go to Step 4; otherwise go to Step 2.
- **Step 4.** Current calculation by Eq. (36).

Figure 2 gives an explicit illustration of the above work flow.

III.E Model parameter selection

III.E.1 The selection of non-electrostatic potential

Non-electrostatic effects are important to ion conductance efficiency. Unfortunately, it is expensive to give a full quantitative description for U_{Nonelec}. In current existing models, such as PNP based ones, the U_{Nonelec} is integrated as an overall effect and represented implicitly by the phenomenologically reduced diffusion coefficients in the channel pore region. While in BD based models, the effect of U_{Nonelec} exists in the ion friction factor, which is also related to the diffusion coefficient by Einstein's relation.[35] All these treatments indicate that U_{Nonelec} should be related to the diffusion coefficient of ions, which is a physical observable. Based on this discussion, we ignore all detailed components while describe the non-electrostatic interactions as one effective, overall component in the mean field manner. As indicated by Eq. (12), the U_{Nonelec} is also a density functional of the $n(\mathbf{r})$, and the first term represents the connection between U_{Nonelec} and given reference ion density. It is quite obvious that α is a tunable parameter. Here we focus on how to choose parameter $V_{\mathrm{Ion-sur}}$.

For a simple start, let this energy be related to the relaxation time τ of an ion by $V_{\mathrm{Ion-sur}} = \hbar/2\tau$, according to the Einstein's relation $D = k_B T\tau/m$, where D and m are the diffusion coefficient and mass of the particle. Then the energy $V_{\mathrm{Ion-sur}}$ can be given by

$$V_{\mathrm{Ion-sur}} = \frac{\hbar k_B T}{2mD} \tag{84}$$

for protons. With appropriate the proton mass and the diffusion coefficient in the bath, one yields $V_{\mathrm{Ion-sur}} \approx 3.4 k_B T$. However, the value of diffusion coefficient in the channel is commonly believed reduced, but is inconclusive due to the variation of the channel pore structure diameters and solvation conditions. According to Table 1 of Ref.,[20] proton diffusion coefficients reduce to 1/2 to 1/7 of that in the bath condition in various lipid layers. We take the resulting reduction accordingly in the channel region. This argument gives the U_{Nonelec} a range of $6k_B T \sim 20k_B T$.

III.E.2 Choices of the dielectric constants

The Poisson equation describes the electrostatic potential function due to existence of free charges. The left hand side of the Poisson equation can be written as

$$-\nabla^2 \Phi(\mathbf{r}) + \nabla \cdot P(\mathbf{r}) \tag{85}$$

$P(\mathbf{r})$ is the polarization field vector which describes the density of permanent or induced electric dipole moments in a dielectric material. For an isotropic medium that has linear response, the polarization field can be defined by

$$P(\mathbf{r}) = \chi E(\mathbf{r}) = -\chi \nabla \Phi(\mathbf{r}) \tag{86}$$

where $\chi(\mathbf{r}) = \epsilon(\mathbf{r}) - 1$ is the dielectric susceptibility of the medium. Then Eq. (85) can be written as

$$-\nabla \cdot \epsilon(\mathbf{r}) \nabla \Phi(\mathbf{r}). \tag{87}$$

Therefore, the permittivity $\epsilon(\mathbf{r})$, which is also called dielectric constant, represents the polarizability of the medium. In biomolecular calculations, $\epsilon(\mathbf{r})$ is generally assumed as piecewise constants in most applications. It is noted that in charge neutral molecules, electric polarization corresponds to the rearrangement of electrons in molecules. In most popular force field packages, some of the polarizations of a charge neutral macromolecule are often treated as partial charges located at the centers of individual atoms. These partial charges give rise to most of the fixed charge source term ρ_f in the generalized Poisson-Boltzmann equation. Due to this treatment of the polarization effect, a relatively small $\epsilon(\mathbf{r})$ value is normally assigned to the biomolecular domain. For example, when calculating the solvation energy of proteins, $\epsilon(\mathbf{r})$ is set to 1 or 2 for the biomolecular domain while 80 for the solvent domain. These values are commonly accepted and vary in only small ranges for different purposes. However, in the application of ion channels, choices of dielectric constants in different regions of interest are worthwhile to be carefully explored.

First, although the ion permeation is a dynamical process, dielectric constants are all assumed time independent due to fact that the electrolytic solution is a fast relaxing bath, i.e., the relaxation time of the solvent water is extremely short. Secondly, the dielectric constants are approximated as piecewise constants for computational simplicity. In the bulk concentration, a widely used dielectric constant as 80, which is the experimental measurement at room temperature for water. The value of ϵ is usually set to 1 or 2 in the protein domain, which partially accounts for the field-induced atomic polarization of the protein. However, two features about protein structures are neglected in the continuum approximation for ion channels and should be partially compensated by the dielectric constant of the channel protein. One is the re-organization of the protein and water in extremely confined channels and the other is the protein's response to ion's presence in the channel, since the ion permeation takes places at the same time scale. Therefore, in order to encapsulate these features in a continuum model with a single dielectric coefficient, the value of $\epsilon(\mathbf{r})$ for channel proteins is suggested to be greater than 2.

There are also some issues in assigning the dielectric coefficient for the aqueous region in the ion channel. A general conclusion is that $\epsilon(\mathbf{r})$ in the bulk aqueous region should be much higher that

that in the channel region. The main reason is the high confinement of the channel geometry. In ion channel pores which are usually very narrow, water molecules are highly ordered, and their motions are restricted, so are their response to external fields. Therefore, the value of $\epsilon(\mathbf{r})$ should be much smaller than 80, and can be as small as 3 for a dry channel pore. However, these extreme value do not work well in practical computations. In fact, the dielectric coefficient in the channel pore region is still taken as 80 in most existing models despite the above arguments. In the present work, $\epsilon(\mathbf{r})$ values are set to be smaller than 80, but are not too small in order to model the biological environment.

III.E.3 Effective mass of the proton

The choice of effective mass $m(\mathbf{r})$ of the particle in the total Hamiltonian H as in Eq. (21) is an important issue to be discussed. The concept of effective mass origins from the solid state physics, which describes the response of the charge carrier to the electric or magnetic fields when quantum mechanism is applied. It is defined by analogy with Newton's second law but in the quantum mechanical framework

$$m = \hbar^2 \left[\frac{d^2 E}{dk^2} \right]^{-1} \tag{88}$$

where E and k are the energy and the corresponding wavenumber of the particle, respectively. Generally the effective mass is chosen in the range of 0.001 or 10 times the real mass of the particle and depends on the material and the experimental condition. However, little research has been done, to our knowledge, on the choice of the effective mass of protons in proton channels or proton experiments. In the present model, we describe protons by quantum mechanics while treat many other particles by classical mechanics and/or continuum description. Therefore, an effective mass approximation is appropriate for our model. We set effective mass $m(r)$ as a model parameter and its value is chosen from 0.01 to 1.0 time of the real proton mass.

III.E.4 Normalization of the proton density

The integration of the density function $n(\mathbf{r})$ of protons is constrained by the total number of protons in the system

$$\int_{\Omega_s} n(\mathbf{r}) d\mathbf{r} = N_p, \tag{89}$$

where $n(\mathbf{r})$ satisfies the governing Kohn-Sham equation and N_p should be a known quantity. However, in most experimental set-ups, one does not know N_p. Instead, the bulk concentration or the bulk number density, n_p^0, is given. When the solvent domain is sufficiently large compared to the channel pore region, one has two approximations

$$N_p \cong n_p^0 \int_{\Omega_s} e^{-q(\Phi(\mathbf{r}) - V_{\mathrm{Ext}})/k_B T} d\mathbf{r} \cong n_p^0 \int_{\Omega_s} d\mathbf{r}, \tag{90}$$

where the second approximation is a crude estimation.

IV Numerical simulations

In this section, the validity of the proposed model and related performance analysis are presented based on a specific channel protein, Gramicidin A (GA, PDB code: 1MAG). The GA channel protein is obtained from the soil bacterial species Bacillus brevis and is one of the best studied molecular channels, both structurally and functionally. In a bilayer membrane, the GA is dimers and consists of two head-to-head β-helical parts. Each part of the dimer has the sequence of FOR-VAL-GLY-ALA-DLE-ALA-DVA-VAL-DVA-TRP-DLE-TRP-DLE-TRP-DLE-TRP-ETA, and forms a narrow pore of about 4Å in diameter and 25Å in length. It appears to select small monovalent cations while reject multivalent ions, both cations and anions. In our approach, the GA structure is downloaded from the PDB, and the pdb file is processed by the PDB2PQR,[22] in which the radii and partial charges are adopted from the CHARMM force field values.[36] The molecular surface of the GA is generated via the MSMS package[47] with water probe radius 1.3 Å and density 10. Figure 3 gives an illustration of the GA in a 3D display of the structure, surface and electrostatics distribution. From Fig. 3(a), one can see that a complete channel pore is formed after the generation of the molecular surface. Although the GA is neutral in general, its surface electrostatics

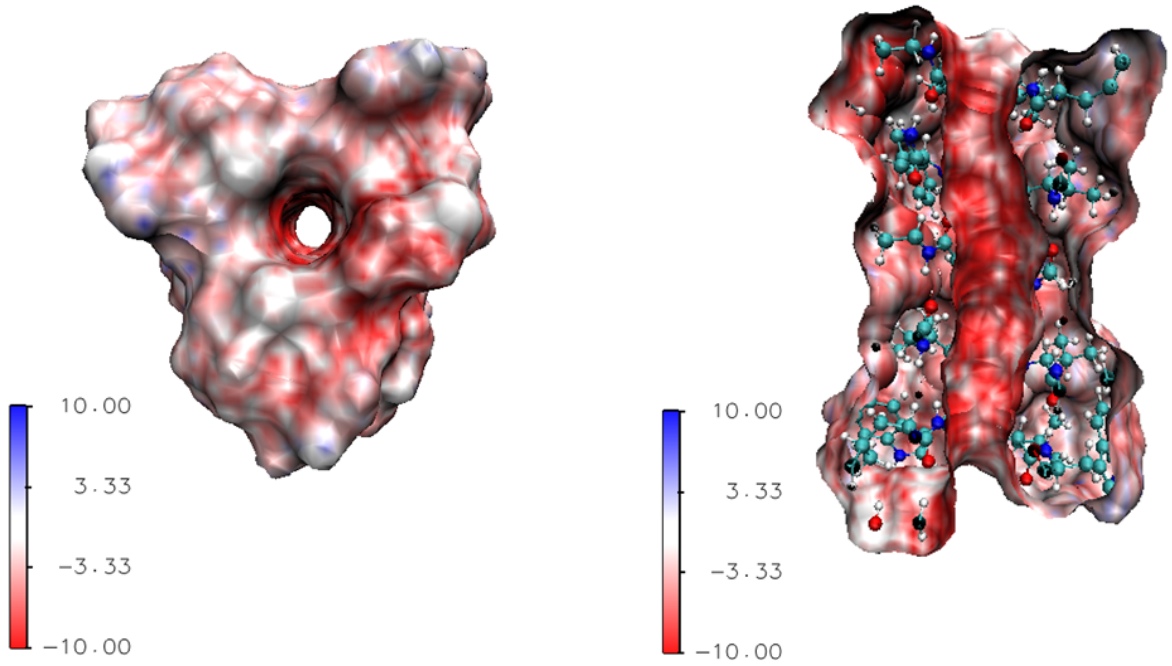

(a) (b)

Figure 3: 3D illustration of the Gramicidin A channel structure and surface electrostatic potential. The negative surface electrostatics as indicated by the intensive red color on the channel upper surface and inside the channel pore implies that the GA selects positive ions. (a) Top view of the channel; (b) Side view of the channel.

is negatively distributed near the channel mouth as indicated by the red color. Furthermore, as shown in Fig. 3(b), the inner part of the channel pore is also intensively negatively charged. This fact indicates the selectivity of GA channel to positive ions. Having prepared the GA structure and surface, the channel pore is aligned to z-direction. The simulation grid resolution is taken as 0.5Å. Under this discretization all the grid points are classified as either in the solvent domain or in the molecular domain. Furthermore, the molecular surface is projected on each layer along the transport direction to determine the beginning and the end of the channel respectively by the first layer and the last layer on which closed projections can be found. An artificial membrane slab is added along the transport direction between the beginning and end of the channel, see Fig. 1(b).

IV.A Electrostatic properties of the Gramicidin A channel

This subsection presents the electrostatic analysis of the GA channel over a wide range of $\epsilon(\mathbf{r})$ values in the present model. At the atomic level, the motion of an ion when it is passing through the channel is determined by a number of factors, such as electrostatic interactions and non-electrostatic interactions. The electrostatic interactions include the Columbic interactions between ions, and between ions and fixed charges of the channel. The non-electrostatic interactions consist of ion-ion excluded volume effects, the thermal fluctuation of the solvent, van der Waals interactions, and other short range interactions such as the frequent collisions and associations between water molecules and ions. One more factor is the structural cooperation of the channel protein during ion permeation. In the present model, the quantitative description of electrostatic interactions is the major ingredient while the degrees of freedom of non-electrostatic interactions are suppressed to reduce the computational cost.

The electrostatics of the channel system depends on the dielectric constants. In the present work, we carefully test the effect of dielectric constants within an appropriate biological range in order to obtain

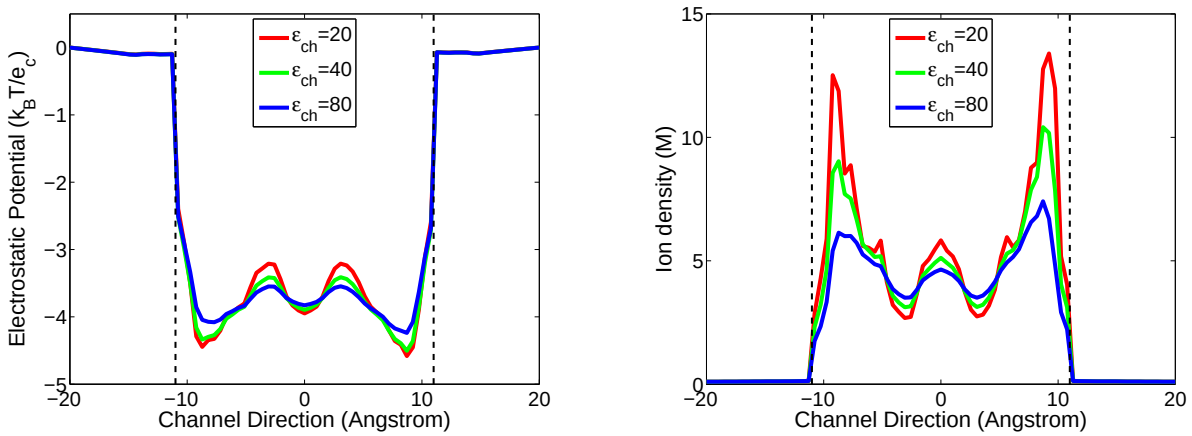

(a) Electrostatics (b) Ion density

0

Figure 4: Electrostatic potential and charge density of the GA channel along the z-axis obtained with $\epsilon_m = 2$ and $n_p^0 = 0.1$ molar (Red: $\epsilon_{\rm ch} = 20$; Green: $\epsilon_{\rm ch} = 40$; Blue: $\epsilon_{\rm ch} = 80$). (a) Electrostatic potential profiles in channel; (b) Proton density profiles in the channel.

a reasonable prediction. It is also worth checking the dependence or changing trend of the electrostatics upon these parameters for model training and validity verification. Before the transport problem is simulated, the mathematical algorithms, choices of dielectric constants are carefully examined via the generalized Poisson-Boltzmann equation.

As discussed earlier, $\epsilon_m(\mathbf{r})$ is given as constant in Ω_m and its value is tested over a range. However, $\epsilon_s(\mathbf{r})$ is strongly position dependent, having different values in the bulk solvent and the channel pore. For simplicity, we take $\epsilon_s(\mathbf{r})$ as piecewise constant, i.e., impose a constant value denoted as $\epsilon_{\rm bath}$ in the bulk solvent, whereas another for the channel pore denoted as $\epsilon_{\rm ch}$. There is no controversy upon the choice of $\epsilon_{\rm bath} = 80$, which is employed in all the following simulations. Figures 4-6 display the electrostatic potential profiles and (positive) ion density in GA protein with various combinations of $\epsilon_{\rm ch}$ and ϵ_m within the range discussed in the earlier section. The reference ion density is taken as 0.1 molar.

All quantities in Figs. 4-6 are averaged on each cross section along the channel axis. The vertical dash lines in these figures indicate the entrance (left) and exit (right) of the channel. The GA protein is overall neutral in charge, but possesses a negative environment in the channel region and this fact leads to potential well. Near the entrance and the exit of the channel, there are two local potential minima (the valley near the dash line) and a major barrier in the middle of the channel. Accordingly, for the density profile, there are two peaks at the positions where two energy minima present and the density is lower in the middle of the channel. These electrostatic profiles agree with the biological properties of the GA channel.

For each fixed ϵ_m, the magnitude of the electrostatic potentials responds directly to the change of $\epsilon_{\rm ch}$ value, as showed in Fig. 4(a). When the $\epsilon_{\rm ch}$ decreases from 80, which is the commonly used value for the solvent, to the lower values suggested by biological observations, the contrast between the energy wells near the entrance/exit and the barrier in the middle becomes sharper. This phenomenon verifies the impact of $\epsilon_{\rm ch}$ value and leads us to prefer the lower value in our model. For the ion density profile shown in Fig. 4(b), the changes in the peaks with respect to the changes of $\epsilon_{\rm ch}$ are very clear. As $\epsilon_{\rm ch}$ doubles, the magnitudes of the density at the peaks decrease half accordingly.

The impact of ϵ_m can be examined by fixing $\epsilon_{\rm ch}$, i.e., checking the same color curves throughout Figs. 4-6. It can be found out that changes in ϵ_m do not affect the potential structure but solely change the magnitudes. When ϵ_m increases, the absolute value of electrostatic potential decreases, and consequently the proton density becomes smaller.

Figure 7 depicts the electrostatics profile change with respect to reference proton densities at a certain

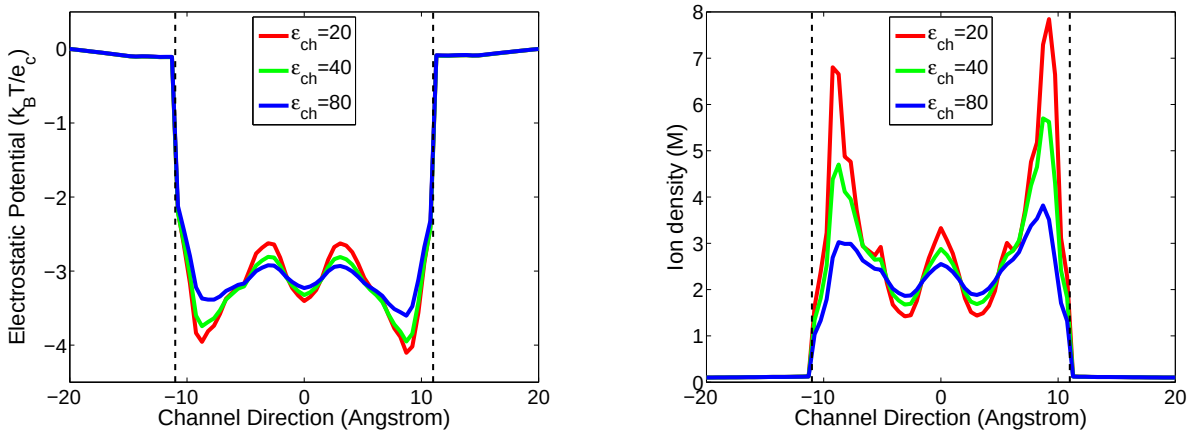

(a) Electrostatics (b) Ion density

Figure 5: Electrostatic potential and charge density of the GA channel along the z-axis obtained with $\epsilon_m = 5$ and $n_p^0 = 0.1$ molar (Red: $\epsilon_{\rm ch} = 20$; Green: $\epsilon_{\rm ch} = 40$; Blue: $\epsilon_{\rm ch} = 80$). (a) Electrostatic potential profiles in channel; (b) Proton density profiles in the channel.

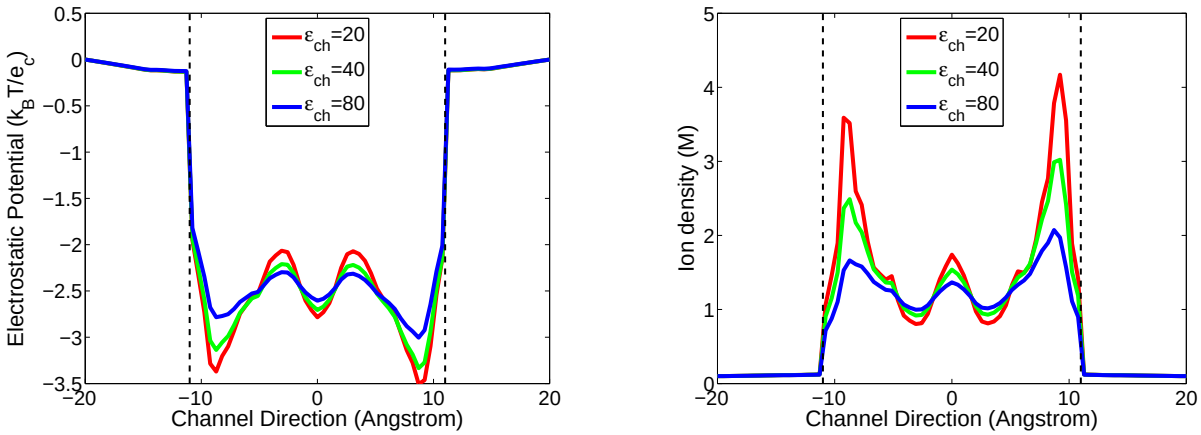

(a) Electrostatics (b) Ion density

Figure 6: Electrostatic potential and charge density of the GA channel along the z-axis obtained with $\epsilon_m = 10$ and $n_p^0 = 0.1$ molar (Red: $\epsilon_{\rm ch} = 20$; Green: $\epsilon_{\rm ch} = 40$; Blue: $\epsilon_{\rm ch} = 80$). (a) Electrostatic potential profiles in the channel; (b) Proton density profiles in the channel.

combination of dielectric constants ($\epsilon_m = 5$ and $\epsilon_{\rm ch} = 40$). It is easy to see that the higher the proton reference concentration, the higher the sources in the Poisson equation and the results in electrostatic potential profiles are.

IV.B Conductivity properties of the Gramicidin A channel

The mechanism of the selectivity of the GA channel can be easily explained in view of the overall potential landscape. Figure 8 shows the total effective potential with both the electrostatic and non-electrostatic contributions. Since the latter component is described in reduced manner in the present treatment. Figure 8(a) is for the monovalent cautions while Fig. 8(b) is for monovalent anions. According to the previous discussion, the non-electrostatic potential serves as an energy barrier while the GA protein provides a negatively charged environment for cations in the channel region. Two energy components with opposite signs cancel each other and result in an overall potential landscape that permeates

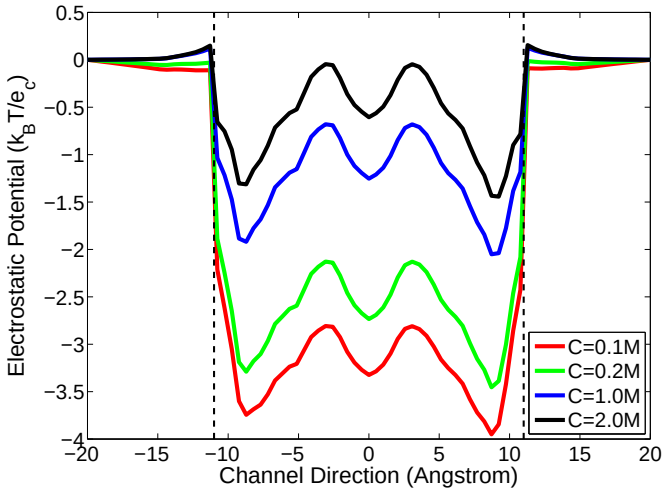

Figure 7: Electrostatic potential profiles of the GA channel under different ion reference densities n_p^0. Red: $n_p^0 = 0.1$ molar; Green: $n_p^0 = 0.2$ molar; Blue: $n_p^0 = 1.0$ molar; Black: $n_p^0 = 2.0$ molar. $\epsilon_m = 5$ and $\epsilon_{\rm ch} = 40$.

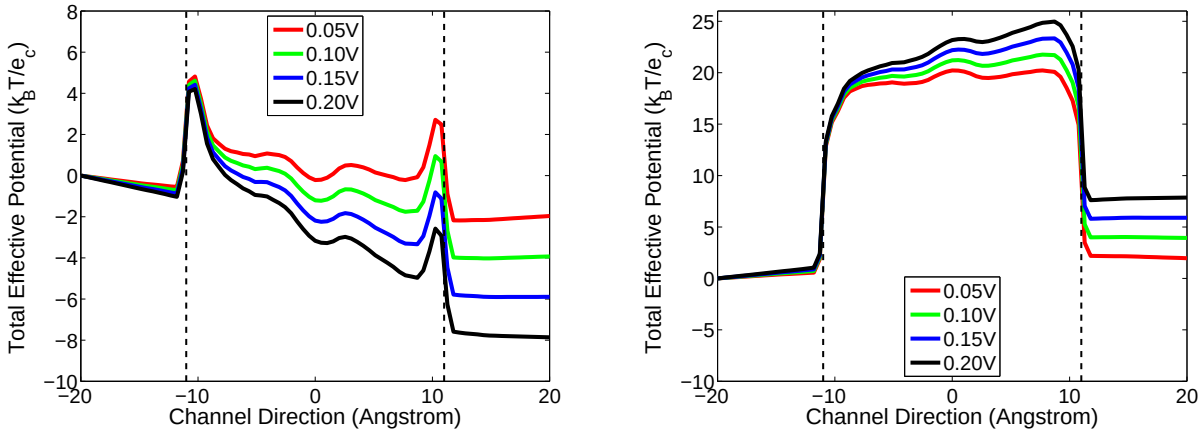

(a) For monovalent cations (b) For monovalent anions

Figure 8: The total potential of the GA channel which includes electrostatic and non-electrostatic contibutions under various voltage biases. Dielectric constants are $\epsilon_m = 5$ and $\epsilon_{\rm ch} = 30$. The pH value of the solution is 2.75. (a) Total potential of monovalent cations; (b) Total potential of monovalent anions.

a monovalent cation. However, the overall potential gives rise to a huge barrier for the anions since the positive non-electrostatic potential adds up with the positive electrostatic potential, as Fig. 8(b) shows.

Conductance reveals the efficiency of the ion channel transport of some specific ions. Due to the fast development of experimental technologies in the past several decades, the single-channel conductance can be measured and becomes one of the prevalent descriptor of the channel function. The simulation of channel conductance mainly focuses on calculating the channel current within the physiological ranges of membrane potentials (i.e., $-0.2\text{V} < V < 0.2\text{V}$) and bath concentrations (up to molars). The channel conducting current is measured at the scale of pico-Ampere (pA) for ion channels. The corresponding characteristics of channel conductance is observed at the scale of pico-Siemens (pS) and is recorded in the voltage-current (I-V) curves and concentration-current (C-C) curves. Based on experimental observations, the I-V curves are expected to be in linear or sub-linear form while the C-C curves are supposed

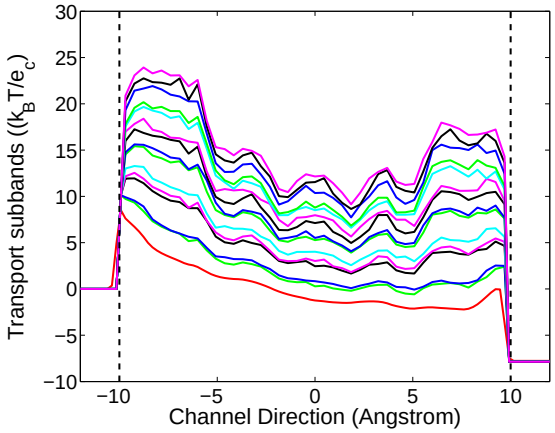

Figure 9: The first 15 eigenvalues (the $U^j(z)$ in Eq. 40) of the effective potentials along the transport direction used in the transport calculations at the voltage bias of 0.2V.

to exhibit saturation behavior, i.e., when the concentration increases, the conductance increases linearly at beginning and then becomes saturated later on.

The conductivity of the proton channel mainly depends on the proton scattering process. Thus we first present the effective potential profile along the transport direction. Figure 9 depicts the first 15 effective potential eigenvalues (i.e., $U^j(z)$ in Eq. (40)) used in the current calculation under the voltage bias of 0.2V. Similarly, the channel region is presented between two black dash lines. The channel region is essentially confined by the protein surface and a tube-like pore is formed. As displayed in Fig. 9, the potential energy profile in the channel pore region has discrete eigenstates, due to the small area confinement at each cross section and the light mass of the proton. For each specific location along the transport direction, the discrete ascending energies correspond to the eigenvalues of the operator in Eq. (39). In theory, the total number of the eigenvalues is infinite, but is finite in practical computations, and depends on the discretization of the cross section. In principle, all the eigenvalues should be accounted in computations. However, numerically, due to the Boltzmann distribution, higher energy components contribute little in the total transport quantity. In practical, only a few low lying eigenvalues need to be included in numerical simulations. In our case, the first 15 eigenstates are sufficient to obtain a good degree of convergence in calculating the proton density and current.

Figure 10 illustrates the simulation results of the present multiscale model for proton transport, compared with the experimental data from the literature[50] for the GA channel. The blue dots in each figure represent the available experimental observations for certain voltage biases while the red curves are our model predictions calculated with sufficiently many voltage samples. The model parameters are chosen to match the experimental data but all of the choices are taken within the range of physical measurements. The dielectric coefficients are taken as $\epsilon_m = 5$, $\epsilon_{\rm ch} = 30$ and $\epsilon_{\rm bath} = 80$, according to the discussion in previous sections. To determine the non-electrostatics the diffusion coefficients of protons are taken as 3.6×10^{-9} m^2/s in the channel, less than a half of the value in the bulk environment, and the relative weighting parameter is set to $\alpha = 0.03$. Taking into account above considerations, we can conclude that experimental data and the present predictions agree quite well and this agreement verifies the validity of our quantum dynamics in continuum model.

Apart from I-V curves, there are also experimental data available about the conductance-concentration relation (C-C curve) of the proton transport under given voltages. Figure 11 displays such a relationship with a comparison between experimental data and model predictions. At a given voltage bias, the conductance of the channel is calculated with various proton concentrations as indicated by the horizontal axis. Using the same set of parameters as those in Fig. 10, the computed conductance-concentration relation also agrees fairly well with experimental data. At lower proton concentrations (i.e., pH value being greater than 2), the agreement between our prediction and experimental data is quite good. At

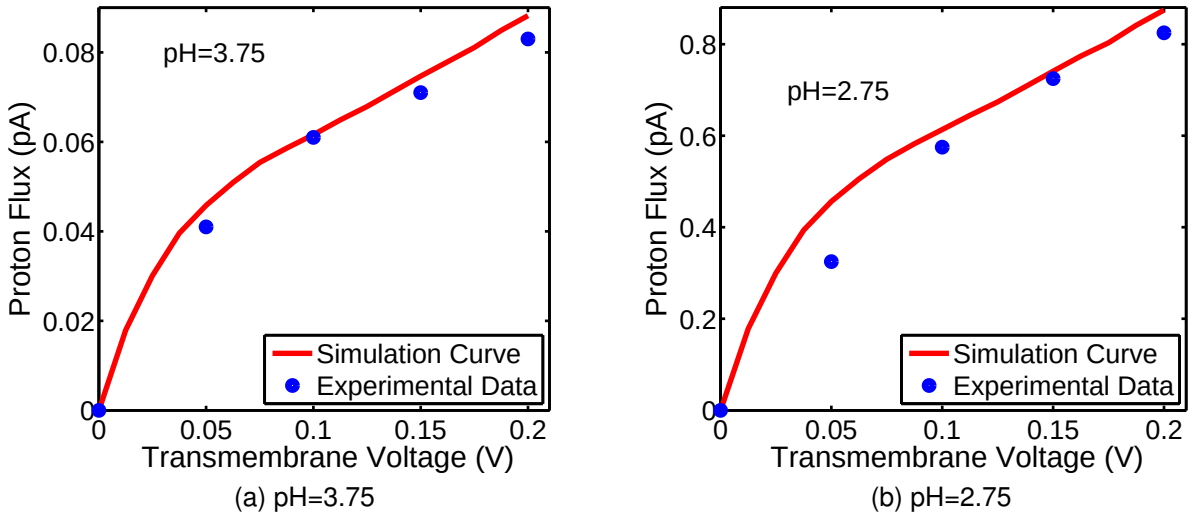

Figure 10: Voltage-current relation of proton translocation of GA at different concentrations. Blue dots: experimental data of Eisenman et al;[26] Red curve: model prediction.

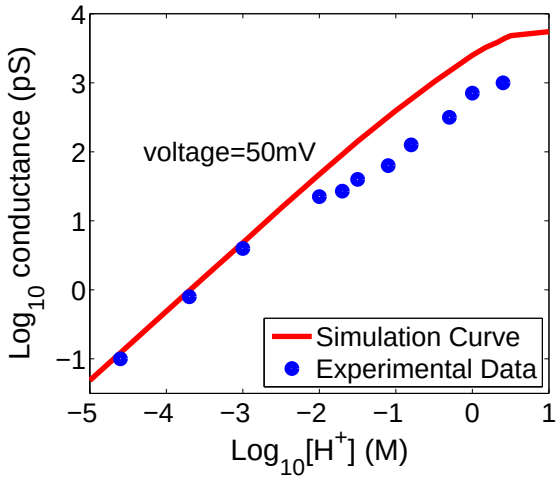

Figure 11: Conductance-concentration relation of proton translocation at a fixed voltage. Voltage bias=0.05V; Blue dots: experimental data of Eisenman et al;[26] Red curve: model prediction.

relatively higher concentrations, although the numerical simulations slightly overestimate the observed conductance, the conductance saturation against the concentration can still be observed in simulations and it corresponds to the sub-linear characteristics or the flat tail of the C-C curve.

The experimental data used in this work are reported by Eisenman et al[26] and are also employed to verify another proton transport model by Schumaker et al.[50] There are other experimental data on proton conductance available[3,14,20] but under different experimental conditions. First, the experimental data provided by Cukierman et al.[20] offer proton conductions recorded with natural Gramicidin A and with its Dioxolane-Linked dimer in different lipid bi-layers (phosphatidylethanolamine-phosphatidylcholine, or PEPC and glycerymonooleate, or GMO). Their experimental studies were carried out for low (9.8 mM) and high (1578 mM) proton concentrations against the transmembrane voltages. Additionally, in another piece of work,[14] the attenuation of proton transfer in Gramicidin water wires by phosphoethanolamine

was investigated and a number of I-V curves were provided. It is impossible to fit all the experimental data by a single group of parameters because of the difference in experimental conditions and lipid membrane types. Nevertheless, it can be observed that our simulation curves under the current set of parameters have shown similar qualitative shapes. Therefore, the present model can fit to these experimental data by slightly adjusting model parameters to reflect the different experimental conditions. Finally, Akeson and Deamer[3] also reported I-V curves of proton conductance for the $\mathrm{F_1F_0}$ATPases studies. In their results, a severe saturating or sublinear character is found for proton concentration of 10 mM and there were an obvious superlinear pattern for 1.0 M hydrogen chloride (HCl). Our model can not capture these characteristics by just tuning the parameter values. In fact, this set of experimental data was also found difficult for another theoretical model of proton transport.[50]

IV.C Model limitations

Based on the multi-scale approximation, the present mode captures the most important factors which have large impacts on the proton permeation. Meanwhile, the quantum treatment of protons provides a potential analysis tool to account for the quantum behavior in proton channel transport and proton translocation in biomolecules. The setup of the present model roots from essential biophysical principles with reasonable approximations, and thus the numerical simulations give considerably good agreements with experimental data under appropriate choices of model parameters. However, this model also has a number of limitations, which are to be studied further in the future. First, in this model, the channel is assumed to be rigid, i.e. it does not response to the permeation of ions. This is not true in real situation and the configuration change of the channel protein has been found to have fairly important impact on the ion permeation process. Although the omitted ion-protein interaction has been somehow compensated implicitly by adjusting the dielectric constants, this interaction can not be fully accounted unless more sophisticated models, such as the multiscale molecular dynamics,[54] are invoked. Additionally, the plasma membrane where the channel protein is embedded is simplified. There are various types of membranes, some of them have dipoles and others have charges. In our model, the membrane is just approximated by the uniformly distributed dielectric medium and the charges or dipole effects are neglected. However, there is no essential difficulty to improve this aspect in our model. Point charges from membranes can be added in the present model. Otherwise, a position dependent dielectric constants for the biomolecular region can also represent the charge effects in the membrane. Finally, the other limitation of the present model is the simplified treatment of non-electrostatic interactions, which reduces the number of the degrees of freedom, although. Compared to the electrostatic potential, the non-electrostatic potential plays a less important role in general. However, it may be of crucial importance for channel selectivity in certain situations. Therefore, an emergent task of our future work is to come up with more quantitative modeling of non-electrostatic interactions meanwhile without significantly increasing the number of degrees of freedom.

V Conclusion

Proton dynamics and transport across membrane proteins are of paramount importance to the normal function of living cells. Although there are a variety of excellent theoretical models and efficient computational methods for ion channels in general, most commonly used models are much less successful when they are applied to the proton channel transport due to the unique characteristics of protons. It is commonly believed that to a certain extent, proton channels demonstrate quantum mechanical properties such as the translocation as shown in the Grotthuss-type mechanism.[2,39] However, the exact role of quantum mechanics in the atomic mechanism of proton channels is still unclear despite of a number of elegant theories in the literature, partly due to the complexity of ion channel systems. The present paper introduces a quantum dynamics in continuum (QDC) model for the prediction and analysis of proton density distribution and conductance in proton channels. Our essential ideas are as follows. First, protons behave quantum mechanically due to their light masses and channel geometric confinement in protein channels. Therefore, a quantum mechanical treatment of protons is necessary. Additionally, since the primary interactions in proton channels are of ion-ion electrostatic type and the van der Waals type of interactions involve less energy, a dielectric continuum treatment of solvent medium may provide a reasonable approximation to the effect of numerous solvent molecules. Most importantly, this treatment

dramatically reduces the dimensionality of the problem. As such, our approach is called a QDC model. Moreover, since the atomic detail of the protein structure serves as a physical boundary for proton dynamics and transport, the present model returns molecular surface to separate the continuum solvent domain from the discrete charge domain of the protein. Finally, densities of all other ions and counterions in the solvent are described by the Boltzmann distribution, which is a quasi-equilibrium description as the electrostatic potential varies during the process of proteins permeating the membrane.

We propose a multiscale variational paradigm to accommodate the aforementioned aspects in a unified framework. The total free energy functional encompasses the kinetic and potential energies of protons, and the electrostatic energies of ions and fixed charges in the channel system. The first variation is carried out via the Euler-Lagrange equation to derive the governing equations for the system. A generalized Poisson-Boltzmann equation is obtained for the electrostatic potential while a generalized Kohn-Sham equation is resulted for the state of protons in the system. The solution to these two coupled nonlinear equations leads to the desirable electrostatic distribution and proton density profile in the channel system. Expressions for proton density and proton flux across the membrane are derived from fundamental principles.

The computation of the proposed coupled equations involves a number of mathematical issues, such as the linearization of coupled nonlinear partial differential equations (PDEs) using the Gummel iterations and/or inexact Newton iterations, and the solution of elliptic PDEs with discontinuous coefficients (i.e., piecewise dielectric constants), singular sources (i.e., Dirac delta functions for protein charges), and nonsmooth interfaces (i.e., geometric singularities). In the present work, we utilize the Dirichlet to Neumann mapping method to take care of singular charges, and the matched interface and boundary (MIB) method to accurately handle the discontinuous coefficients and geometric singularities.

The Gramicidin A (GA) channel protein, a popular protein structure, is employed in our numerical studies to demonstrate the performance of the proposed QDC model. We give a detailed discussion about the rational for model parameter selections. The electrostatic property of the GA channel is analyzed with the proposed model against a large number of model parameters. Proton transport properties, i.e., the current voltage (I-V) curves, are investigated over a large number of combinations of applied voltages and reference bulk concentrations. Our model predictions are compared with experimental data, which validates the present QDC model. Finally, we provide detailed discussion of model limitations and possible future improvements.

Acknowledgments
This work was supported in part by NSF grant CCF-0936830, NIH grant R01GM-090208 and MSU Competitive Discretionary Funding Program grant 91-4600. The authors thank Qiong Zheng for useful discussions.

Literature cited

[1] N. Abaid, R. S. Eisenberg, and W. S. Liu. Asymptotic expansions of I-V relations via a Poisson-Nernst-Planck system. *SIAM Journal on Applied Dynamical Systems*, 7(4):1507–1526, 2008.

[2] N. Agmon. The grotthuss mechanism. *Chem. Phys. Lett*, 244:456–462, 1995.

[3] M. Akeson and D. Deamer. Proton conductance by the gramicidin water wire. Model for proton conductance in the $\mathrm{F_0F_1ATP}$ases? *Biophys J.*, 60:101–109, 1991.

[4] J. Bothma, J. Gilmore, and R. McKenzie. The role of quantum effects in proton transfer reactions in enzymes: quantum tunneling in a noisy environment? *New Journal of Physics*, 12(055002), 2010.

[5] S. Braun-Sand, A. Burykin, Z. T. Chu, and A. Warshel. Realistic simulations of proton transport along the gramicidin channel: Demonstrating the importance of solvation effects. *J. Phys. Chem. B*, 109:583–592, 2005.

[6] M. Burger, R. S. Eisenberg, and E. Heinz. Inverse problems related to ion channel selectivity. *SIAM J Applied Math*, 67(4):960–989, 2002.

[7] A. E. Cardenas, R. D. Coalson, and M. G. Kurnikova. Three-dimensional poisson-nernst-planck theory studies: Influence of membrane electrostatics on gramicidin a channel conductance. *Biophysical Journal*, 79:80–93, July 2000.

[8] D. Chen, Z. Chen, C. Chen, W. H. Geng, and G. W. Wei. MIBPB: A software package for electrostatic analysis. *J. Comput. Chem.*, in press, 2010.

[9] D. Chen and G. W. Wei. Modeling and simulation of nano-electronic devices. *J. Comput. Phys.*, 229:4431–4460, 2010.

[10] D. Chen and G. W. Wei. Multi-scale modeling and simulation for proton trans-location in the ion channel, in Workshop on Fluid Motion Driven by Immersed Structures, Fields Institute, Toronto. August 9-13 2010.

[11] H. Chen, Y. Wu, and G. Voth. Proton transport behavior through the influenza a M2 channel: Insights from molecular simulation. *Biophys J.*, 93:3470–3479, 2007.

[12] Z. Chen, N. A. Baker, and G. W. Wei. Differential geometry based solvation models I: Eulerian formulation. *J. Comput. Phys.*, 2010.

[13] Z. Chen, N. A. Baker, and G. W. Wei. Differential geometry based solvation models II: Lagrangian formulation. *J. Math. Biol.*, 2010.

[14] A. Chernyshev and S. Cukierman. Proton transfer in gramicidin water wires in phosphlipid bilayers: Attenuation by phosphoethanolamine. *Biophys J.*, 91:580–587, 1997.

[15] S.-H. Chung, T. Allen, and S. Kuyucak. Conducting-state properties of the kcsa potassium channel from molecular and brownian dynamics simulations. *Biophysical Journal*, 82:628–645, 2002.

[16] S.-H. Chung and S. Kuyucak. Recent advances in ion channel research. *Biochimica et Biophysica Acta*, 1565:267–286, 2002.

[17] B. Corry, S. Kuyucak, and S.-h. Chung. Test of poisson-nernst-planck theory in ion channels. *The Rockefeller University Press*, 114(4):597–599, October 1999.

[18] B. Corry, S. Kuyucak, and S.-H. Chung. Dielectric self-energy in Poisson-Boltzmann and Poisson-Nernst-Planck models of ion channels. *Biophysical Journal*, 84:3594–3606, June 2003.

[19] R. Cukier. Theory and simulation of proton-coupled electron transfer, hydrogen-atom transfer, and proton translocation in proteins. *Biochimica Et Biophysical Acta-Bioenergetics*, 1655:37–44, 2004.

[20] S. Cukierman, E. P. Quigley, and D. S. Crumrine. Proton conduction in gramicidin a and in its dioxolane-linked dimer in different lipid bilayers. *Biophys J.*, 73:2489–2502, 1997.

[21] C. de Falco, J. W. Jerome, and R. Sacco. A self-consitent iterative scheme for the one-dimensional steady-state transistor calculations. *IEEE Trans. Ele. Dev.*, 11:455–465, 1964.

[22] T. J. Dolinsky, J. E. Nielsen, J. A. McCammon, and N. A. Baker. PDB2PQR: An automated pipeline for the setup, execution, and analysis of Poisson-Boltzmann electrostatics calculations. *Nucleic Acids Research*, 32:W665–W667, 2004.

[23] W. Dyrka, A. T. Augousti, and M. Kotulska. Ion flux through membrane channels: An enhanced algorithm for the Poisson-Nernst-Planck model. *J. Comput Chem*, 29:1876–1888, 2008.

[24] S. Edwards, B. Corry, S. Kuyucak, and S.-H. Chung. Continuum electrostatics fails to describe ion permeation in the gramicidin channel. *Biophysical Journal*, 83:1348–1360, September 2002.

[25] B. Eisenberg. Ion channels as devices. *Journal of Computational Electronics*, 2:245–249, 2003.

[26] G. Eisenman, B. Enos, J. Hagglund, and J. Sandbloom. Gramicidin as an example of a single-filing ion channel. *Ann. N.Y. Acad. Sci.*, 339:8–20, 1980.

[27] W. Geng, S. Yu, and G. W. Wei. Treatment of charge singularities in implicit solvent models. *Journal of Chemical Physics*, 127:114106, 2007.

[28] M. K. Gilson, M. E. Davis, B. A. Luty, and J. A. McCammon. Computation of electrostatic forces on solvated molecules using the Poisson-Boltzmann equation. *Journal of Physical Chemistry*, 97(14):3591–3600, 1993.

[29] P. Graf, M. G. Kurnikova, R. D. Coalson, and A. Nitzan. Comparison of dynamic lattice monte carlo simulations and the dielectric self-energy Poisson-Nernst-Planck continuum theory for model ion channels. *J. Phys. Chem. B*, 108:2006–2015, 2004.

[30] B. Hille. *Ionic Channels of Excitable Membranes*. Sunderland, MA: Sinauer Associates, 1992.

[31] U. Hollerbach, D. P. Chen, and R. S. Eisenberg. Two- and three-dimensional poisson-nernst-planck simulations of current flow through gramicidin a. *Journal of Scientific Computing*, 16(4):373–409, Decemeber 2002.

[32] H. Hwang, G. C. Schatz, and M. A. Ratner. Ion current calculations based on three dimensional poisson-nernst-planck theory for a cyclic peptide nanotube. *Journal of Physical Chemistry B*, 110:6999–7008, 2006.

[33] Y. W. Jung, B. Z. Lu, and M. Mascagni. A computational study of ion conductance in the kcsa k+ channel using a Nernst-Planck model with explicit resident ions. *J. Chem. Phys.*, 131(215101), 2009.

[34] L. Krishtalik. The mechanism of the proton transfer: An outline. *Biochimica Et Biophysical Acta-Bioenergetics*, 1458:6–27, 2000.

[35] S. Kuyucak, O. S. Andersen, and S.-H. Chung. Models of permeation in ion channels. *Rep. Prog. Phys*, 64:1427–1472, 2001.

[36] J. MacKerell, A. D., D. Bashford, M. Bellot, J. Dunbrack, R. L., J. D. Evanseck, M. J. Field, S. Fischer, J. Gao, H. Guo, S. Ha, D. Joseph-McCarthy, L. Kuchnir, K. Kuczera, F. T. K. Lau, C. Mattos, S. Michnick, T. Ngo, D. T. Nguyen, B. Prodhom, I. Reiher, W. E., B. Roux, M. Schlenkrich, J. C. Smith, R. Stote, J. Straub, M. Watanabe, J. Wiorkiewicz-Kuczera, D. Yin, and M. Karplus. All-atom empirical potential for molecular modeling and dynamics studies of proteins. *Journal of Physical Chemistry B*, 102(18):3586–3616, 1998.

[37] A. B. Mamonov, R. D. Coalson, A. Nitzan, and M. G. Kurnikova. The role of the dielectric barrier in narrow biological channels: A novel composite approach to modeling single-channel currents. *Biophysical Journal*, 84:3646–3661, June 2003.

[38] B. Moy, B. Corry, S. Kuyucak, and S.-H. Chung. Tests of continuum theories as models of ion channels. I. Poisson-Boltzmann theory versus Brownian dynamics. *Biophys. J.*, 78:2349–2363, 2000.

[39] J. Nagle and H. Morowitz. Molecular mechanisms for proton transport in membranes. *Proc. Natl. Acad. Sci. U.S.A*, 1458(72):298–302, 1978.

[40] D. Perlman, D. Case, J. Caldwell, W. Ross, T. Cheatham, S. Debolt, D. Ferguson, G. Seibel, and P. Kollman. Amber, a package of computer programs for applying molecular mechanics, normal mode analysis, molecular dynamics and free energy calculations to simulate the structural and energetic properties of molecules. *Comp. Phys. Commun.*, 91:1–41, 1995.

[41] R. Pomes and B. Roux. Theoretical study of H^+ translocation along a model proton wire. *J. Phys. Chem*, 100:2519–2527, 1996.

[42] R. Pomes and B. Roux. Molecular mechanism of H^+ conduction in the single-file water chain of the gramicidin channel. *Biophysical Journal*, 82:2304–2316, 2002.

[43] R. Pomes and B. Roux. Structure and dynamics of a proton wire: A theoretical study of H^+ translocation along the single-file water chain in the gramicidin a channel. *Biophysical Journal*, 71:19–39, 2002.

[44] B. Roux. Influence of the membrane potential on the free energy of an intrinsic protein. *Biophysical Journal*, 73:2980–2989, December 1997.

[45] B. Roux. Computational studies of the gramicidin channel. *Acc. Chem. Res.*, 35:366–375, 2002.

[46] B. Roux, T. Allen, S. Berneche, and W. Im. Theoretical and computational models of biological ionchannels. *Quarterly Reviews of Biophysics*, 7(1):1–103, 2004.

[47] M. F. Sanner, A. J. Olson, and J. C. Spehner. Reduced surface: An efficient way to compute molecular surfaces. *Biopolymers*, 38:305–320, 1996.

[48] M. Saraniti, S. Aboud, and R. Eisenberg. The simulation of ionic charge transport in biological ion channels: an introduction to numerical methods. *Reviews in Computational Chemistry*, 22:229–294, 2006.

[49] J. R. Schnell and J. J. Chou. Structure and mechanism of the M2 proton channel of influenza a virus. *Nature*, 451:591–596, January 2008.

[50] M. F. Schumaker, R. Pomes, and B. Roux. A combined molecular dynamics and diffusion model of single proton conduction through gramicidin. *Biophysical Journal*, 79:2840–2857, December 2000.

[51] K. A. Sharp and B. Honig. Electrostatic interactions in macromolecules - theory and applications. *Annual Review of Biophysics and Biophysical Chemistry*, 19:301–332, 1990.

[52] A. Singer, D. Gillespie, J. Norbury, and R. Eisenberg. Singular perturbation analysis of the steady state poisson-nernst-planck system: applications to ion channels. *European Journal of Applied Mathematics*, 19:541–560, 2008.

[53] M. S. Till, T. Essigke, T. Becker, and G. M. Ullmann. Simulating the proton transfer in gramicidin a by a sequential dynamical monte carlo method. *J. Phys. Chem*, 112:13401–13410, 2008.

[54] G. W. Wei. Differential geometry based multiscale models. *Bulletin of Mathematical Biology*, 72:1562 – 1622, 2010.

[55] S. Yu and G. W. Wei. Three-dimensional matched interface and boundary (MIB) method for treating geometric singularities. *Journal of Computational Physics*, 227:602–632, 2007.

[56] S. Yu, Y. Zhou, and G. W. Wei. Matched interface and boundary (MIB) method for elliptic problems with sharp-edged interfaces. *Journal of Computational Physics*, 224(2):729–756, 2007.

[57] Q. Zheng, D. Chen, and G. W. Wei. Second-order poisson nernst-planck solver for ion channel transport. *Journal of Comput. Phys.*, 2010.

[58] Y. C. Zhou, M. Feig, and G. W. Wei. Highly accurate biomolecular electrostatics in continuum dielectric environments. *Journal of Computational Chemistry*, 29:87–97, 2008.

[59] Y. C. Zhou, S. Zhao, M. Feig, and G. W. Wei. High order matched interface and boundary method for elliptic equations with discontinuous coefficients and singular sources. *Journal of Computational Physics*, 213(1):1–30, 2006.